MANCHESTER 1824
The University of Manchester

The University of Manchester Research

PTEN reduces endosomal PtdIns(4,5)P2 in a phosphatase-independent manner via a PLC pathway

DOI:
10.1083/jcb.201805155

Document Version
Accepted author manuscript

Link to publication record in Manchester Research Explorer

Citation for published version (APA):
Mondin, V. E., Ben El Kadhi, K., Cauvin, C., Jackson-Crawford, A., Bélanger, E., Decelle, B., Salomon, R., Lowe, M., Echard, A., & Carréno, S. (2019). PTEN reduces endosomal PtdIns(4,5)P2 in a phosphatase-independent manner via a PLC pathway. *The Journal of cell biology*, *218*(7), 2198–2214. https://doi.org/10.1083/jcb.201805155

Published in:
The Journal of cell biology

Citing this paper
Please note that where the full-text provided on Manchester Research Explorer is the Author Accepted Manuscript or Proof version this may differ from the final Published version. If citing, it is advised that you check and use the publisher's definitive version.

General rights
Copyright and moral rights for the publications made accessible in the Research Explorer are retained by the authors and/or other copyright owners and it is a condition of accessing publications that users recognise and abide by the legal requirements associated with these rights.

Takedown policy
If you believe that this document breaches copyright please refer to the University of Manchester's Takedown Procedures [http://man.ac.uk/04Y6Bo] or contact uml.scholarlycommunications@manchester.ac.uk providing relevant details, so we can investigate your claim.

OPEN ACCESS

Download date:30. Jun. 2022

A PTEN/PLC pathway reduces endosomal PI(4,5)P_2 and can compensate for loss of the OCRL phosphatase

Virginie E. Mondin[1,*], Khaled Ben El Kadhi[1,*], Clothilde Cauvin[3,4], Anthony Jackson – Crawford[6], Emilie Bélanger[1], Barbara Decelle[1], Rémi Salomon[5], Martin Lowe[6,$], Arnaud Echard[3,#] and Sébastien Carréno [1,2,&]

[1]Institute for Research in Immunology and Cancer (IRIC), Université de Montréal, P.O. Box 6128, Station Centre-Ville, Montréal, QC H3C 3J7, Canada.

[2]Université de Montréal, Département de Pathologie et de Biologie Cellulaire, Montréal, Québec H3C 3J7, Canada.

[3] Membrane Traffic and Cell Division Lab, Institut Pasteur, UMR3691, CNRS, 25–28 rue du Dr Roux, F-75015 Paris, France.

[4] Sorbonne Université, Collège doctoral, F-75005 Paris, France.

[5]Institut des Maladies Génétiques Imagine, Hôpital Necker - Enfants Malades, Université Paris Descartes, 149, rue de Sèvres F-75015 Paris, France.

[6]Faculty of Biology, Medicine and Health, University of Manchester, Manchester, M13 9PT, UK.

[*] These authors contributed equally to this work.

[#] Corresponding author for the experiments in human cells: arnaud.echard@pasteur.fr

[$] Corresponding author for the experiments in zebra fish: martin.p.lowe@manchester.ac.uk

[&]Corresponding author: sebastien.carreno@umontreal.ca

Abstract

The tumor suppressor PTEN dephosphorylates PtdIns(3,4,5)P_3 into PtdIns(4,5)P_2. Here, we make the unexpected discovery that in Drosophila, PTEN reduces PtdIns(4,5)P_2 levels on endosomes, independently of its phosphatase activity. This new PTEN function requires the enzymatic action of dPLCXD, an atypical Phospholipase C. Importantly, we discovered that this novel PTEN/dPLCXD pathway can compensate for dOCRL depletion, a PtdIns(4,5)P_2 phosphatase. Mutation of OCRL1, the human orthologue of dOCRL, causes Oculocerebrorenal syndrome of Lowe, a rare multisystemic genetic disease. Both OCRL1 or dOCRL loss have been shown to promote accumulation of PtdIns(4,5)P_2 on endosomes and cytokinesis defects. Here, we show that PTEN or dPLCXD overexpression prevents these defects. In addition, we found that chemical activation of this pathway restores normal cytokinesis in human Lowe syndrome cells and rescues OCRL phenotypes in a zebrafish Lowe syndrome model. Our findings identify, a novel PTEN/dPLCXD pathway that controls PtdIns(4,5)P_2 levels on endosomes. They also point to a potential new strategy for the treatment of Lowe syndrome.

Introduction

Phosphoinositides (PtdIns) are lipids composed by a membrane associated diacylglycerol backbone linked to a cytoplasmic inositol ring. Phosphoinositides regulate a number of cellular processes including cell growth, survival, intracellular trafficking and cell morphogenesis (Balla, 2013, Cauvin and Echard, 2015). There are 7 different phosphoinositides obtained by phosphorylation of the 3rd and/or 4th and/or 5th position of their inositol ring (Fig. 1A). More than 100 kinases, phosphatases and phospholipases control the levels of phosphoinositides directly on membranes (Balla, 2013, Ilmonen et al., 2005). However, how these enzymes collaborate to control homeostasis of the different pools of phosphoinositides is poorly understood.

Dysregulation of phosphoinositide abundance or distribution can lead to numerous pathologies including cancer and genetic diseases (Viaud et al., 2016). For instance mutation of the inositol polyphosphate-5-phosphatase OCRL1 is responsible for the oculocerebrorenal Lowe syndrome and Dent-2 disease, two rare multisystemic orphan diseases (Mehta et al., 2014, De Matteis et al., 2017, Pirruccello and De Camilli, 2012). Patients suffering from these diseases present with neurological defects, congenital cataracts, weak muscle tone, life threatening kidney abnormalities and have a reduced life expectancy. There is no cure for these diseases and the therapeutic treatments available only alleviate some symptoms.

We and others have previously reported that depletion of OCRL1 or depletion of dOCRL, its Drosophila orthologue, causes several characteristic phenotypes: Abnormal accumulation of PtdIns(4,5)P_2 on endosomes, disorganization of the endocytic compartments and cytokinetic defects (Carim et al., 2019, Ben El Kadhi et al., 2012, Ben El Kadhi et al., 2011, Cauvin et al.,

2016, Choudhury et al., 2005, Dambournet et al., 2011, Erdmann et al., 2007, Ungewickell et al., 2004, Vicinanza et al., 2011, Del Signore et al., 2017, Nandez et al., 2014, De Leo et al., 2016). In control cells, PtdIns(4,5)P_2 concentrates at the cortical equator (Emoto et al., 2005, Field et al., 2005, Roubinet et al., 2011) and recruits the cytokinetic machinery that allows subsequent cytokinesis (Ben El Kadhi et al., 2011, Liu et al., 2012, Cauvin and Echard, 2015). We previously found that by dephosphorylating PtdIns(4,5)P_2 into PtdIns(4)P, both OCRL1 and dOCRL play important roles during cell division in human and Drosophila cells respectively. As observed for OCRL1 in human cells, we previously reported that dOCRL localizes on endosomes where it reduces the levels of PtdIns(4,5)P_2 (Ben El Kadhi et al., 2011). We also showed that dOCRL dsRNA depletion promotes accumulation of PtdIns(4,5)P_2 on endosomes in interphase and triggers the appearance of aberrant enlarged endosomal compartments. In anaphase, this abnormal intracellular accumulation of PtdIns(4,5)P_2 recruits the cytokinetic machinery at the expense of the equatorial plasma membrane. As a result, furrowing and cytokinesis are defective and cells present a high rate of multinucleation (Ben El Kadhi et al., 2011). Thus, the cytokinetic defects observed upon dOCRL depletion are a secondary consequence of the dysregulation of PtdIns(4,5)P_2 levels on endosomes. In human cells depleted for OCRL1, or in Lowe syndrome patient cells harboring a mutation of the OCRL gene, PtdIns (4,5)P_2 accumulation on endosomes is less pronounced (Cauvin et al., 2016, Nandez et al., 2014, Vicinanza et al., 2011) and multinucleation is barely observed (Dambournet et al., 2011). Nevertheless, we showed that at the end of cytokinesis OCRL1 plays a role in removing PtdIns(4,5)P_2 at the plasma membrane of the intercellular bridge, which allows proper abscission of the two daughter cells (Dambournet et al., 2011). In OCRL1 depleted cells and in

renal Lowe patient cells, we indeed found an important delay in the duration of abscission. In addition, using a zebrafish model of Lowe syndrome, we also reported that OCRL1 inactivation triggers endocytic defects in the pronephric tubule (Oltrabella et al., 2015). This phenotype is reminiscent of the renal tubulopathy observed in patients with Lowe syndrome (Bockenhauer et al., 2008).

The initial objective of the present study was to understand how PtdIns(4,5)P_2 is produced on endosomes of dOCRL-depleted cells. We previously identified two enzymes important for direct production of PtdIns(4,5)P_2 in Drosophila S2 cells: Skittles, a kinase that phosphorylates PtdIns(4)P to produce PtdIns(4,5)P_2 and PTEN, a tumor suppressor phosphatase that dephosphorylates PtdIns(3,4,5)P_3 into PtdIns(4,5)P_2 (Roubinet et al., 2011). Here, we make the unexpected discovery that PTEN also reduces levels of PtdIns(4,5)P_2 on endosomes. Moreover, overexpression of an enzymatic dead mutant of PTEN rescues phenotypic defects of dOCRL-depleted cells. We further show that this new function of PTEN depends on the phospholipase C, dPLCXD. In an attempt to stimulate this new PTEN/PLCXD pathway to rescue dOCRL depletion, we used *m*-3M3FBS, a small molecule that directly activates PLCs (Bae et al., 2003). Treatment of Drosophila cells with *m*-3M3FBS corrects the cytokinetic defects observed upon dOCRL depletion, dependently of dPLCXD but independently of PTEN. Finally to assess if the chemical activation of PLCs could be used as a new therapeutic strategy to treat Lowe syndrome, we tested *m*-3M3FBS in two other models of Lowe syndrome. The activator of PLCs rescues the cytokinetic defects in human cells depleted for OCRL1 and in renal cells from Lowe syndrome patient. We finally show that *m*-3M3FBS rescues OCRL1 depletion *in vivo,* by restoring endocytosis in the pronephric tubule of a Lowe syndrome zebrafish model.

RESULTS:

PTEN prevents the effects of dOCRL depletion independently of its phosphatase activity.

PtdIns(4,5)P_2 is mainly restricted to the plasma membrane where it controls several important functions (Kolay et al., 2016). In addition, PtdIns(4,5)P_2 is also present on other compartments such as endosomes and lysosomes (Vicinanza et al., 2011, Yoshida et al., 2017, De Leo et al., 2016). We wanted to assess if the PtdIns4P-kinase Skittles or the PtdIns(3,4,5)P3 phosphatase PTEN were responsible for the high PtdIns(4,5)P_2 levels on the enlarged endosomes observed upon dOCRL depletion(Ben El Kadhi et al., 2011) (Fig. 1A).

We first expressed a GFP version of Skittles (Roubinet et al., 2011) and we observed that in addition to the plasma membrane this kinase localized on endomembranes (Fig S1A). In dOCRL-depleted cells, Skittles also localized on the large abnormal endomembrane compartment typically observed after dOCRL depletion (Fig. 1B). In addition overexpression of Skittles further increased the extent of multinucleation in dOCRL-depleted cells while its overexpression alone did not significantly alter these levels in control S2 cells (Fig. 1C and S1B). This suggests that Skittles, by producing PtdIns(4,5)P_2 on endomembranes, further increased PtdIns(4,5)P_2 endosomal levels caused by dOCRL depletion. As a result, Skittles overexpression triggered a higher rate of cytokinesis failure. According to this hypothesis, we found that depleting Skittles together with dOCRL reduced the levels of multinucleation compared to the sole depletion of dOCRL (Fig. S1C). This shows that a balance of Skittles and dOCRL activities regulates PtdIns(4,5)P_2 on endomembranes and cytokinesis outcome.

In addition to the plasma membrane, PTEN has been localized to endosomes (Naguib et al., 2015, Shinde and Maddika, 2016). Thus we postulated that modulation of PTEN function would give similar outcomes to the ones observed with Skittles. We found that PTEN depletion did not affect cytokinesis efficiency (Fig. S1D). However, we unexpectedly observed a strong reduction of multi-nucleated cells when PTEN was overexpressed in dOCRL-depleted cells (Fig. 1B & C). We also found that this function of PTEN does not rely on its catalytic activity. Expression of a phosphatase dead mutant of the enzyme (Maehama and Dixon, 1998), $PTEN_{C132S}$, also significantly reduced the levels of multinucleation observed upon dOCRL depletion (Fig. 1B & C). Since the cytokinetic defect of dOCRL-depleted cells is a consequence of the accumulation of PtdIns(4,5)P_2 on endomembranes, we next tested whether $PTEN_{C132S}$ prevented multinucleation by restoring normal PtdIns(4,5)P_2 localization. We measured PtdIns(4,5)P_2 changes by quantitative microscopy using a PtdIns(4,5)P_2 reporter S2 cell line that we characterized previously (Ben El Kadhi et al., 2011, Roubinet et al., 2011). This cell line stably expresses low levels of Tubby-GFP, a specific biosensor of PtdIns(4,5)P2 (Quinn et al., 2008). We already reported that Tubby-GFP faithfully probes alterations of PtdIns(4,5)P_2 localization between the endomembranes and the plasma membrane (Ben El Kadhi et al., 2011, Roubinet et al., 2011). Using this model we quantified what we thereafter refer to as the PtdIns(4,5)P_2 homeostasis ratio by calculating the proportion of Tubby-GFP on endomembranes over the plasma membrane (Ben El Kadhi et al., 2011, Szentpetery et al., 2009). This ratio is lower in control cells than in dOCRL-depleted cells reflecting the increase of PtdIns(4,5)P_2 on endosomes (Fig. 1D & E, and (Ben El Kadhi et al., 2011)). We found that in dOCRL-depleted cells, overexpression of $PTEN_{C132S}$ restored the PtdIns(4,5)P_2 homeostasis ratio to levels comparable

to control cells (Fig. 1D & E). This suggests that PTEN can lower levels of PtdIns(4,5)P_2 on endosomes in dOCRL-depleted cells independently of its phosphatase activity .

The PBD and C2 domains of PTEN are necessary and sufficient to prevent the effects of dOCRL depletion.

To better understand how PTEN overexpression rescue dOCRL loss, we performed a structure-function analysis. PTEN comprises five conserved domains (Worby and Dixon, 2014) (Fig. 2A), a N-terminal phosphoinositide binding domain (PBD) that binds to PtdIns(4,5)P_2, a catalytic domain, a C2 domain known to promote binding to various lipids and proteins, an auto-inhibitory C-tail domain and a C-terminal PDZ binding motif mediating protein-protein interaction. We individually deleted PTEN -PBD, -catalytic, -C2 and -C-tail/PDZ domains and measured the ability of each mutant to prevent cytokinesis failure upon dOCRL depletion. We first observed that the catalytic domain of PTEN was dispensable for rescue of cytokinesis failure in dOCRL-depleted cells, confirming that PTEN functions in this context independently of its phosphatase activity (Fig. 2B & S2A). All constructs were expressed at comparable levels, but only the mutants missing the PBD or the C2 domains did not rescue the cytokinetic defects seen upon dOCRL depletion. This demonstrates that these domains are both necessary to rescue the phenotypes caused by dOCRL loss (Fig. 2B & Fig. S2B). We then tested if they were sufficient by constructing a chimera between the PBD and C2 domains of PTEN ($PTEN_{PBD\text{-}C2}$). We found that expression of $PTEN_{PBD\text{-}C2}$ prevented cytokinesis failure in dOCRL-depleted cells while expression of the PBD or the C2 domain of PTEN alone did not (Fig. 2B & C). As observed with expression of

$PTEN_{C132S,}$ the expression of $PTEN_{PBD-C2}$ is also sufficient to rescue a normal PtdIns(4,5)P_2 homeostasis ratio in dOCRL-depleted cells (Fig. 2D). Remarkably, when expressed in a control background, we observed that $PTEN_{PBD-C2}$ or $PTEN_{C132S}$ reduces the PtdIns(4,5)P_2 homeostasis ratio suggesting that their overexpression promotes a decrease of PtdIns(4,5)P_2 levels on endomembranes independently of dOCRL status (Fig. 2E). These results suggest a broad role of PTEN in modulating PtdIns(4,5)P_2 levels on endomembranes.

PTEN controls PtdIns(4,5)P_2 levels on endosomes.

In human cells, PTEN was reported to localize to endosomes and to bind to Rab7, a marker of late endosomes (Naguib et al., 2015, Shinde and Maddika, 2016). We first aimed to assess if PTEN localized to this compartment in Drosophila S2 cells. We probed PTEN localization using $PTEN_{C132S}$ or $PTEN_{PBD-C2}$ to minimize possible perturbation of phosphoinositide composition and identity of the endosomal compartments by activity of PTEN, which dephosphorylates PtdIns(3,4,5)P_3. In accordance with a role for PTEN in reducing PtdIns(4,5)P_2 levels on endocytic compartments, we found that these two forms of PTEN partially co-localized with Rab7 and the recycling endosome marker Rab 11 (Fig. 3A,B, S3A & B). In addition, PTEN constructs partially co-localized with the LysoTracker probe that marks acidic organelles such as late endosomes and lysosomes (Majzoub et al., 2016) (Fig. 3C & S3C).

We then depleted PTEN in control cells to test whether this protein controlled PtdIns(4,5)P_2 levels on endomembranes. In contrast to $PTEN_{PBD-C2}$ or $PTEN_{C132S}$ overexpression, PTEN depletion increased the PtdIns(4,5)P_2 homeostasis ratio (Fig. 3D), suggesting an increase of

PtdIns(4,5)P_2 on endomembranes. Accordingly, we observed, upon PTEN depletion, an increase in the number of cells with cytoplasmic vesicles marked by the PtdIns(4,5)P_2 biosensor, Tubby-GFP (Fig. 3D & E). Since we found that PTEN localizes to endosomes, we asked if these PtdIns(4,5)P_2 rich vesicles were endocytic compartments. For this, we incubated PTEN dsRNA Tubby-GFP cells with the LysoTracker probe and we found a partial co-localization of the PtdIns(4,5)P_2 biosensor with LysoTracker (Fig. 3F & S3D). All together, these results bring to light a new function of PTEN in controlling PtdIns(4,5)P_2 levels on endosomes.

A PLC activity is required downstream of PTEN to rescue dOCRL depletion.

Since $PTEN_{C132S}$ and $PTEN_{PBD\text{-}C2}$ do not have any enzymatic activity we reasoned that to control PtdIns(4,5)P_2 levels on endosomes, PTEN requires another enzyme that can directly act upon PtdIns(4,5)P_2 (Fig 1A). Some of the most efficient enzymes that hydrolyze PtdIns(4,5)P_2 are enzymes of the phospholipase C (PLC) family. PLCs hydrolyze the phosphodiester bond between the phosphorylated inositol ring of PtdIns(4,5)P_2 and the diacylglycerol backbone (Kadamur and Ross, 2013). We thus tested whether PTEN can rescue dOCRL depletion through the enzymatic activity of a PLC. To this aim, we expressed $PTEN_{C132S}$ or $PTEN_{PBD\text{-}C2}$ while inhibiting all PLC enzymes using U73122, a cell-permeable pan-PLC inhibitor (Smith et al., 1990). This inhibitor did not cause cytokinetic defects by itself, but it prevented both PTEN constructs from rescuing cytokinesis defects caused by dOCRL depletion (Fig. 4A and 4B). This demonstrates that PTEN requires a downstream PLC activity in order to rescue dOCRL depletion.

dPLCXD acts downstream of PTEN to rescue dOCRL depletion.

We then aimed to identify which Drosophila PLC acted downstream of PTEN. We co-depleted 5 different PLC enzymes together with dOCRL in S2 cells and quantified multinucleation after $PTEN_{PBD\text{-}C2}$ expression. The individual depletion of each PLC did not cause cytokinesis defects in control cells (Fig. S4A). Among the 5 PLCs tested, we found that only the depletion of CG14945 prevented $PTEN_{PBD\text{-}C2}$ from rescuing the cytokinetic defects triggered by dOCRL depletion (Fig. 5A & S4B). We named this enzyme, dPLCXD, as it is the Drosophila ortholog of three human PLCXD (Gellatly et al., 2012) (Fig. 5B & C). To confirm that dPLCXD can rescue dOCRL loss, we expressed dPLCXD in dOCRL-depleted cells. We first found that, as its human orthologs PLCXD-1 and PLCXD-3 (Gellatly et al., 2012), dPLCXD localized to endomembranes and not to the plasma membrane (Fig. 5D). Similarly to what we observed with PTEN overexpression, we found that overexpression of dPLCXD is sufficient to rescue multinucleation in dOCRL-depleted cells (Fig. 5E). The enzymatic domain of PLCXDs contains two catalytic histidine residues critical for their enzymatic activity that are conserved from bacteria to human (Fig 5C and (Essen et al., 1997, Heinz et al., 1995, Gellatly et al., 2012)). To test if the phospholipase activity of dPLCXD was necessary to prevent the consequences of dOCRL depletion, we constructed an enzymatic dead mutant, dPLCXD(HL)2, by mutating these conserved catalytic histidines (219 and 277 in dPLCXD) into leucines (Fig. 5C). In control cells, dPLCXD(HL)2 overexpression did not modify the rate of multinucleation (Fig. S4C). However, while still localized on endomembranes, dPLCXD(HL)2 could not prevent multinucleation when expressed in dOCRL-depleted cells (Fig. 5D and E). This demonstrates that dPLCXD prevents cytokinesis failure via its enzymatic activity. These results

reveal that, to reduce PtdIns(4,5)P_2 levels on endosomes, PTEN requires the enzymatic action of dPLCXD.

dPLCXD controls PtdIns(4,5)P_2 levels on endosomes.

To further understand the role of dPLCXD in the control of PtdIns(4,5)P_2 homeostasis, we first determined the identity of the endomembranes to which dPLCXD localizes (Fig. 5D). We found that, as observed for PTEN, dPLCXD also associated with late and recycling endosomes, as marked by Rab7 and Rab11 respectively (Fig. 6A,B, S3E & F). To assess whether, as seen for PTEN, dPLCXD regulated PtdIns(4,5)P_2 levels on endosomes of control cells, we depleted this phospholipase and investigated the distribution of PtdIns(4,5)P_2 using the biosensor Tubby-GFP. In accord with a new PTEN/dPLCXD pathway regulating PtdIns(4,5)P_2 levels on endosomes, the depletion of dPLCXD caused PtdIns(4,5)P_2 to accumulate on endomembranes (Fig. 6D & E). dPLCXD-depleted cells showed an increase of the PtdIns(4,5)P_2 homeostasis ratio together with a higher number of cells with cytoplasmic vesicles marked by the PtdIns(4,5)P_2 biosensor, Tubby-GFP (Fig. 6C & D). Furthermore, we found that many of the PtdIns(4,5)P_2 vesicles were positive for the marker of late endosomes and lysosomes LysoTraker (Fig. 6F & S3G). Altogether these results identify a new function of dPLCXD in controlling PtdIns(4,5)P_2 on endosomes.

PTEN acts through dPLCXD to rescue dOCRL depletion.

Having shown that both PTEN and dPLCXD regulate PtdIns(4,5)P_2 on endosomes and can rescue dOCRL depletion, we then aimed to better understand how they functionally interact. We first assessed the co-localization of PTEN and dPLCXD and found that $PTEN_{PBD\text{-}C2}$ or $PTEN_{C132S}$ partially co-localize with dPLCXD on cytoplasmic vesicles of S2 cells (Fig. 7A & S3H). We then tested whether PTEN and dPLCXD physically associate within cells. After co-expression of $PTEN_{PBD\text{-}C2}$ and dPLCXD with various tags, we did not observe any interaction of these proteins by conventional co-immunoprecipitation or by GFP-trap (data not shown). This suggests that while they co-localize, PTEN and dPLCXD do not physically interact, or that their interaction is too weak or transient to be detected by these methods.

We then tested whether PTEN is necessary for dPLCXD to rescue dOCRL loss. Upon PTEN depletion, expression of dPLCXD was no longer sufficient to rescue multinucleation of dOCRL-depleted cells (Fig. 7B). This shows that dPLCXD requires PTEN upstream in order to prevent the consequences of dOCRL depletion. PTEN could act via dPLCXD by controlling its endosomal recruitment, or by activating its phospholipase function. Since we observed that dPLCXD still localizes to endomembranes when PTEN is depleted (Fig. 7C), we favor the second hypothesis.

Chemical activation of PLC prevents defects caused by dOCRL depletion

We demonstrated that dPLCXD catalytic activity was necessary to rescue the phenotypes caused by dOCRL depletion (Fig. 5D and E). We thus hypothesized that we could compensate for dOCRL loss by chemically activating the enzymatic function of PLCs. We decided to test this hypothesis by comparing the action of *m*-3M3FBS, a chemical activator of every PLC, with that

of its inactive stereoisomer *o*-3M3FBS (Bae et al., 2003). We found that treatment of dOCRL-depleted S2 cells with the PLC activator *m*-3M3FBS restored the PtdIns(4,5)P_2 homeostasis ratio to that similar to control cells (Fig. 8 A & B). In addition, we found that while *m*-3M3FBS did not perturb cytokinesis in control cells, it reduced the rate of multinucleated cells in dOCRL-depleted cells (Fig. 8 C & D). In contrast, treatment with the inactive analog, *o*-3M3FBS gave only a moderate effect on the PtdIns(4,5)P_2 homeostasis ratio and multinucleation in dOCRL-depleted cells, possibly due to residual activity of this analog on Drosophila PLCs (Fig. 8A, B, C & D).

In addition, we found that in S2 cells the chemical activator of PLCs rescues dOCRL depletion by specifically activating dPLCXD. When dPLCXD was co-depleted together with dOCRL, *m*-3M3FBS could no longer rescue the multinucleation caused by dOCRL depletion (Fig. 8E). Thus, since *m*-3M3FBS directly stimulates PLC activity *in vitro* (Bae et al., 2003), we asked if PTEN was still required when dPLCXD is chemically activated. In the absence of PTEN, *m*-3M3FBS was still able to reduce the rate of multinucleation upon dOCRL depletion (Fig. 8F). This demonstrates that PTEN stimulation of dPLCXD can be bypassed by the direct chemical activation of dPLCXD phospholipase activity. In line with what we proposed in the previous paragraph, this further suggests that PTEN activates dPLCXD phospholipase function (Fig. 9).

Chemical activation of PLC prevents defects observed in different models of Lowe syndrome.

We then tested whether activation of PLCs by *m*-3M3FBS could be used for correcting the defects associated with OCRL1 inactivation in other models for Lowe syndrome. To test this

hypothesis we first analyzed the consequences of *m*-3M3FBS treatment in human Lowe syndrome cell models. We previously reported that cytokinetic abscission is delayed both upon depletion of OCRL1 by RNAi in HeLa cells, and in renal epithelial cells of a Lowe patient harbouring an inactive version of OCRL1 (Dambournet et al., 2011). Importantly, the abscission delay observed in Lowe patient cells was fully corrected by treatment with *m*-3M3FBS, but not by inactive *o*-3M3FBS (Fig. 10A & B). However, *m*-3M3FBS did not change the timing of abscission in normal cells (renal cells collected from a healthy donor). We confirmed these results in HeLa cells treated with control and OCRL siRNAs (Fig S5 A & B). We conclude that the abscission delay resulting from OCRL inactivation or depletion is corrected by low doses of the PLC activator *m*-3M3FBS.

Finally, to test whether activation of PLCs can rescue phenotypes induced by depletion of OCRL1 in an *in vivo* context we used a previously established zebrafish model for Lowe syndrome (Ramirez et al., 2012). This model, which is deficient in OCRL1, has a renal tubular endocytosis defect which can be attributed to excessive accumulation of PtdIns(4,5)P_2 (Oltrabella et al., 2015). To determine if activation of PLCs can rescue the endocytic defect in Lowe syndrome zebrafish, we treated either embryos with *m*-3M3FBS or the inactive analog *o*-3M3FBS and monitored accumulation of injected endocytic tracer in the renal tubule as assessed by fluorescence microscopy (Fig. 10C). Remarkably, *m*-3M3FBS treatment had no effect on renal uptake in wild-type embryos, but efficiently rescued endocytosis in the renal tubule of OCRL1 mutant embryos (Fig. 10D). The inactive analog had no effect in either zebrafish strain. These results indicate that chemical activation of PLCs can rescue loss of OCRL1

function in an *in vivo* context, namely the renal tubule, one of the major tissues affected in Lowe syndrome patients.

DISCUSSION

In this study we discovered a new signaling pathway by which PTEN controls levels of PtdIns(4,5)P_2 on endosomes, which is dependent upon the phospholipase activity of dPLCXD. We then demonstrated that overexpression of members of this new PTEN/dPLCXD signaling pathway can rescue dOCRL depletion in Drosophila cells. Finally, by further characterizing this pathway, we identified a new potential therapeutic strategy that can alleviate the consequences of OCRL1 loss: We showed that treatment with *m*-3M3FBS, a small molecule that activates PLCs, rescues OCRL1 functional loss in three different *in-cellulo* and *in-vivo* models of Lowe syndrome.

A new PTEN/dPLCXD signaling pathway controls PtdIns(4,5)P_2 levels on endosomes.

The vast majority of studies on PTEN have explored its role within the PI3K pathway at the plasma membrane, or in the nucleus. Only recently, a few studies have investigated the role of PTEN on endomembranes. PTEN was recently shown to associate with endosomes, and to dephosphorylate Rab 7 to modulate endosome maturation and EGFR trafficking (Shinde and Maddika, 2016). Our findings confirm that in Drosophila, PTEN localizes on endosomes. In addition we shed light on a novel role for PTEN in controlling PtdIns(4,5)P_2 levels on

endosomes, as demonstrated by the increase of PtdIns(4,5)P_2 on these structures when PTEN is depleted. This finding is further supported by the decrease of PtdIns(4,5)P_2 homeostasis ratio observed when a catalytically inactive mutant of PTEN ($PTEN_{PBD\text{-}C2}$ or $PTEN_{C132S}$) is expressed in cells.

We also found that this new function of PTEN requires the downstream phospholipase activity of dPLCXD. While typical PLC enzymes harbor a catalytic domain composed of a separate X- and Y-box, members of the PLCXD family contain only the X-box (Gellatly et al., 2012). Yet, the three human PLCXD paralogs have been shown to promote hydrolysis of phosphoinositides in cells (Gellatly et al., 2012). Our findings confirm that, as its human orthologs PLCXD-1 and PLCXD-3 (Gellatly et al., 2012), dPLCXD also localizes to endomembranes, which we identify here as endosomes. Importantly, since dPLCXD is not associated with the plasma membrane, the PTEN/dPLCXD pathway must be at play only on endosomes. Besides subcellular localization and tissue expression, there is little information on the cellular roles of PLCXDs. Hence, we have discovered the first function for a member of this family by establishing that dPLCXD controls PtdIns(4,5)P_2 levels on endosomes.

We have established this new role for PTEN after the surprising discovery that overexpression of this tumor suppressor restores normal PtdIns(4,5)P_2 homeostasis, and downstream cytokinesis defects, in dOCRL-depleted cells. By combining studies in wild-type and in dOCRL-depleted cells, we have obtained a set of experimental evidence to define this novel PTEN/dPLCXD signaling pathway. We found that (i) PTEN and dPLCXD partially co-localize on endomembranes (Fig. 7A & S3H); (ii) PTEN or dPLCXD depletion both promote enrichment of PtdIns(4,5)P_2 on endosomes (Fig. 3D,E,F,G and 6C,D,E,F). (iii) dPLCXD acts downstream of PTEN

(Fig. 5A); (iv) dPLCXD catalytic activity is necessary to rescue cytokinesis defects in dOCRL-depleted cells (Fig. 5D,E); (v) dPLCXD requires an upstream action of PTEN to rescue dOCRL depletion (Fig. 7B); (vi) PTEN is not necessary for dPLCXD endomembrane localization (Fig. 7C) and (vii) dPLCXD activation by m-3M3FBS bypasses the requirement for PTEN to rescue dOCRL depletion (Fig. 8F). Altogether these results lead us to propose a model whereby PTEN regulates dPLCXD activation to control PtdIns(4,5)P_2 levels on endosomes (Fig. 9). Since m-3M3FBS also rescues OCRL1 loss both in human cells and zebrafish embryos, it suggests that the role of PLCXD phospholipases on endosomal PtdIns(4,5)P_2 is conserved across species.

The precise molecular mechanism that allows PTEN to stimulate dPLCXD activation remains to be identified. We did not detect any physical interaction by co-immunoprecipitation between the proteins, suggesting that any interaction is too weak or transient to be detected by this method, or that others proteins transmit the signal from PTEN to dPLCXD. Further characterization of the proteins that interact with both dPLCXD and PTEN may therefore provide information as to how PTEN and dPLCXD functionally interact. Interestingly, we showed that a minimal chimera composed of the PBD and C2 domains of PTEN reduces PtdIns(4,5)P_2 levels on endomembranes in dOCLR-depleted cells. While the tumor suppressor role of PTEN is mainly attributed to its PtdIns(3,4,5)P_3 phosphatase activity, some studies have shown that PTEN can also function independently of its catalytic activity (Song et al., 2012). For instance, PTEN was shown to regulate cell migration independently of its phosphatase activity (Raftopoulou et al., 2004), through its C2 domain. Here, we show that the PBD and C2 domains of PTEN are necessary and sufficient to restore PtdIns(4,5)P_2 homeostasis in dOCRL depleted cells. The PBD domain of PTEN is known to bind to PtdIns(4,5)P_2. C2 domains are found in more

than 100 proteins and are known to mediate membrane binding through phospholipid interaction (Corbalan-Garcia and Gomez-Fernandez, 2014). In addition, they have also been shown to directly bind to phosphotyrosine motifs, as for the C2 domain of the serine/threonine Protein Kinase C delta (Benes et al., 2005), or to mediate protein-protein interaction, as for the C2 domain of synaptotagmins that is responsible of its interaction with syntaxins (Li et al., 1995). Therefore, identification of proteins that specifically interact with the PBD and C2 domains of PTEN will provide valuable information to better understand how PTEN controls dPLCXD activation.

Tight control of PtdIns(4,5)P_2 homeostasis is crucial for several important functions such as cell growth, division and migration. Here we demonstrate that in addition to dephosphorylating PtdIns(3,4,5)P_3 into PtdIns(4,5)P_2, PTEN also reduces the levels of PtdIns(4,5)P_2, its own product, on endosomes. After hydrolysis of PtdIns(4,5)P_2 by PLCs, two second messengers are produced. They both activate several other signaling pathways: inositol 1,4,5-trisphosphate promotes release of calcium from the endoplasmic reticulum, and diacylglycerol activates Protein Kinase C. Therefore, a better understanding of this novel PTEN/dPLCXD pathway will certainly have several important repercussions on how we envision the role of PTEN as a tumor suppressor.

PLC activation can rescue the consequences of dOCRL depletion.

We showed that overexpression of PTEN or dPLCXD is able to rescue the loss of dOCRL in Drosophila cells. However, an important question is to understand why endogenous levels of

PTEN and PLCXD do not compensate for dOCRL depletion in Drosophila cells, or indeed in Lowe syndrome or Dent-2 patients. This could be explained by a difference of abundance and/or subcellular localisation of PTEN and PLCXD *vs* OCRL1. For instance, PTEN and PLCXD could be both expressed but at an insufficient level to be able to fully rescue OCRL1 loss. However, it is important to notice that, to rescue multinucleation of dOCRL-depleted cells, the PLC activator requires endogenous dPLCXD (Fig. 8E). This shows that at its endogenous level, dPLCXD can compensate for dOCRL function when it is chemically activated. Thus another possibility is that the level of enzymatic activity of PLCXD phosphatases is tightly regulated, possibly by PTEN. Interestingly, Dent-2 disease and Lowe syndrome are both caused by loss of OCRL1 activity. However people suffering from Dent-2 disease present a milder phenotype than patients affected by Lowe syndrome (Bokenkamp et al., 2009). This suggests that other differences may affect the ability to compensate for loss of OCRL1 in individuals suffering from Dent-2 disease or Lowe syndrome. In light of our findings, the milder phenotype in Dent-2 disease may arise from different levels of activation of members of the PLCXD family. Therefore a clinical study comparing the relative amounts, localization and potential mutations of PTEN and PLCXDs in tissues affected by the Lowe syndrome *vs* Dent-2 disease will allow a better understanding of these rare genetic diseases.

The Lowe syndrome and Dent-2 disease are incurable rare genetic syndromes and all medical efforts are limited to treating their multiple clinical manifestations. We showed that in Drosophila cells, depletion of the PtdIns4P-kinase, Skittles together with dOCRL totally rescues the cytokinetic defects observed upon dOCRL depletion alone. As already proposed by others (Vicinanza et al., 2011), PtdIns4P 5-kinase specific inhibitors could represent a therapeutic

strategy to treat Lowe syndrome and Dent-2 disease patients. We discover here that chemical activation of PLCs can rescue depletion of OCRL1 in several disease models. The PLC chemical activator used in our study has been already used in a mouse model without signs of toxicity (Kim et al., 2012). Thus, chemical activation of PLCs by m-3M3FBS could also represent a new therapeutic strategy to treat Lowe syndrome and Dent-2 disease patients.

MATERIALS AND METHODS

DNA Constructs

PTEN-GFP, SKTL-GFP and GFP-Rab11 were previously described in (Roubinet et al., 2011, Ben El Kadhi et al., 2011).

$PTEN_{C132S}$-mCherry, $PTEN_{C132S}$-GFP, and PTEN domain mutants were obtained by inverse PCR using high fidelity Phusion polymerase (New England Biolabs) with the following primers:

$PTEN_{C132S}$ Forward 5' TAAAGCTGGAAAGCGCAGAACCGGTACCATGATCTGCG 3',

$PTEN_{C132S}$ Reverse 5' GAGTGCACGGCTACAACATTGGACGAATCTTCC 3',

PTEN-ΔPBD Forward 5' TACAAAGAAAAAGGATACGATTTGG 3',

PTEN-ΔPBD Reverse 5' CATGTTGCTGCAGAATTCCACCACACTGG 3',

PTEN-Δphosphatase Forward 5' TCTGTTCCATATTCGAAAGTAAGCC 3',

PTEN-Δphosphatase Reverse 5' TCTTCGTATACGTTTTTTACTCACTACATTGC 3',

PTEN-ΔC2 Forward 5' TCTAATTTTAGCAATGATGTTCAAGCTGAAGCG 3',

PTEN-ΔC2 Reverse 5' TCTACTTGAACAAACTAGTTTGG 3',

PTEN-ΔCTerm Forward 5' TCTCCGCGGGCCCGGGATCCACCGGTCGCCACC 3',

PTEN-ΔCTerm Reverse 5' TCTCTCTGCCTCAAAAACGATTGAAATC 3'.

dPLCXD cDNA (CG14945 - UniProt-Q9VKC3_DROME) was synthetized by Lifetechnologies and cloned under an actin promotor. It was fused with the V5 tag "GKPIPNPLLGLDST" in C terminal position with a linker "APV".

dPLCXD (HL)2 mutant was obtained after two successive inverse PCR using high fidelity Phusion polymerase (New England Biolab) on dPLCXD-V5 with the following primers :

dPLCXD-H219L Forward 5' TTGACTCCGGCTCCTATCGTCCCAACTTCGATCCG 3',

dPLCXD-H219L Reverse 5' GGGTGCCTGGTATGAAAAGATCTCTCAGACG 3',

dPLCXD-H277L Forward 5' TCGGGATTACAAAACAACGTCCGCTGCAGG 3'

dPLCXD-H277L Reverse 5' GATAGATGAAAAACGGATCGGGTGAGTTTCG 3'.

S2 Cell culture, dsRNA treatment, transfection and Drug treatment:

Drosophila melanogaster S2 cells were grown at 27°C in Schneider's Drosophila medium complemented with 20% FBS, Penicillin and Streptomycin (Invitrogen). For dsRNA knockdown, dsRNA was produced using T7 RiboMax express large scale RNA production system (Promega). dsRNAs were amplified from plasmid or genomic DNA using the following Primers:

PTEN-Reverse 5' TAATACGACTCACTATAGGGAGACAAGGTTTTCAGTCTATCTGG 3',

PTEN-Forward 5' TAATACGACTCACTATAGGGAGATATCCAGCACCGGATAAACTA 3',

dOCRL-Reverse 5' TAATACGACTCACTATAGGGAGAATCGCGTAGATATCCGGCGGC 3',

dOCRL -Forward 5' TAATACGACTCACTATAGGGAGAAAGGACATTGTCAAGGAGCGC 3',

CG14945-Forward 5'TAATACGACTCACTATAGGGAGGAGATTATCATATTTGGACTCAAGG 3',

CG14945-Reverse 5'TAATACGACTCACTATAGGGAGCTCTGGGGTCAGCTCCGCCATATCGG 3',

CG10747-Forward 5' TAATACGACTCACTATAGGGCGCAACAGTTAAACGAACCC 3',

CG10747-Reverse 5' TAATACGACTCACTATAGGGTGATTATCGACAGGTCACGC 3',

CCG3620-Forward 5' TAATACGACTCACTATAGGGAAAAACTGAAGCCTTGGAAAAA 3',

CG3620-Reverse 5' TAATACGACTCACTATAGGGCGAGTATGGGAAATTCTCGG 3',

CG4200-Forward 5' TAATACGACTCACTATAGGGTTGTGCGTGAGATTGATTCAG 3',

CG4200-Reverse 5' TAATACGACTCACTATAGGGATGCCCATTAAATTGATGCC 3',

CG4574-Forward 5' TAATACGACTCACTATAGGGGCCTGCCGGGAGTACACTT 3',

CG4574-Reverse 5' TAATACGACTCACTATAGGGGCAGCTGGTGCATAACCTCT 3'.

For functional experiments, cells were cultured in 24 or 96-well plates (Greiner Bio-One) for 6 days. Cells were treated with 3.5 µg of dsRNA at day 0 and at day 3. 2 days before fixation cells were transfected with the indicated cDNA using Fugene HD (Promega).

For PLC inhibition experiments, cells were treated with 40 µM of U-73122, 24 hours before fixation (Calbiochem). For PLC activation experiments, cells were treated with 25 µM *m*-3M3FBS (Tocris) or its inactive analog *o*-3M3FBS (Tocris) 24 hours before fixation.

Quantification of multinucleation and PtdIns(4,5)P_2 homeostasis ratio:

For quantification of multinucleation cells were fixed using Paraformaldehyde 4% (Alfa Aesar) for 20 minutes. Coverslips were then washed using TBS. Cells were permeabilized and blocked for at least 1hour in TBS containing 0.02% Saponin and 2% BSA (TBS-Saponin-BSA). F-actin was stained using 1/100 Texas-Red™-X Phalloidin (Invitrogen T7471) or 1/50 Alexa Fluor 647 Phalloidin (Invitrogen A22287). dPLCXD-V5 was revealed by immunostaining using a monoclonal anti-V5 antibody (1/1000, Invitrogen R960-25) and a goat Alexa-488 conjugated secondary antibody anti-mouse (1/400, Invitrogen A11017). Coverslips were mounted using

Vectashield with Dapi (Vector Laboratories). To assess multinucleation, at least 300 cells (n>300) were counted manually per condition per N individual experiment unless otherwise specified.

PtdIns(4,5)P_2 homeostasis ratio was described previously(Ben El Kadhi et al., 2011). Briefly, a stable cell line expressing Tubby-GFP was fixed and permeabilized. A rabbit anti GFP antibody (Invitrogen A6455) and a secondary Alexa 488 conjugated antibody (Invitrogen A11070) was used to stain GFP. Images were acquired using a DeltaVision elite microscope (GE) with a 60x planApo Olympus objective and a CoolSnap HQ2 camera (Photometrics) or a Nikon A1R Nikon confocal microscope with 60x / 1.4 Plan Apo VC DIC N2 objective or 100x / 1.4 Plan Apo DIC N2 objective. For the quantification of Tubby-GFP endomembranes/plasma membrane ratio, images were analyzed using ImageJ software (NIH). Tubby-GFP intensity were measured at the plasma membrane and inside the cell of each individual cell and their background were measured and subtracted. Cells positive for Tubby-GFP vesicles were determined manually.
Images were treated using SoftWorx software (GE), ImageJ software (NIH) and Photoshop (Adobe).

Co-localization Immunofluorescence

Drosophila melanogaster S2 cells were plated on Concanavalin A (0.5ug/ul Sigma C2010) coated coverslips for 3 hours. Then cells were fixed using Paraformaldehyde 4% (Alfa Aesar) for 20 minutes and washed using TBS. Cells were permeabilized and blocked for at least 1hour in TBS containing 0.02% Saponin and 2% BSA (TBS-Saponin-BSA). Cells were incubated with primary antibody diluted in TBS-Saponin-BSA overnight at room temperature (RT), washed three times in TBS-Saponin-BSA, and incubated with secondary antibodies diluted in TBS-Saponin-BSA for 1 hour at RT. Cells were washed two times in TBS-Saponin-BSA and a last time in TBS, before being mounted in Vectashield medium with DAPI (Vector Laboratories). Images were taken using a Zeiss confocal microscope LSM880 NLO using a 63x / 1.4 Plan-Apochromat, DIC objectif. Images were treated using ZEN lite software (ZEISS Microscopy), ImageJ software (NIH) and Photoshop (Adobe).

Immunostaining was performed using a mouse anti-Rab7 antibody (1/200, DSHB), a monoclonal anti-V5 (1/1000, Invitrogen R960-25) or a rabbit anti-V5 (1/500, Abcam Ab9116), a goat Alexa-488 conjugated secondary antibody anti-mouse (1/400, Invitrogen A11017), a goat Texas Red conjugated secondary antibody anti mouse (1/200, Invitrogen T862).

Live cell imaging with LysoTracker™

Drosophila melanogaster S2 Cells were plated for 3 hours in 96-well plates (Sensoplate microplate Greiner Bio-One) previously coated with Concanavalin A (0.5ug/ul Sigma C2010). Then cells were incubated for 1 hour with LysoTracker™ Deep Red (Invitrogen L12492) or LysoTracker™ Green DND-26 (Invitrogen L7526) at 75nM. LysoTracker was washed with fresh medium, and images were taken with a Zeiss confocal microscope LSM880 NLO using a 63x /

1.4 Plan-Apochromat, DIC objectif. Images were treated using ZEN lite software (ZEISS Microscopy), ImageJ software (NIH) and Photoshop (Adobe).

Abscission assays in Human cells

The Lowe patient and normal renal cell lines have been established and characterized in reference (Dambournet et al., 2011), after informed consent was obtained from the patient and his parents, in accordance with French law. HeLa cells were grown in DMEM medium (Gibco BRL) supplemented with 10% fetal bovine serum, 100 U/ml penicillin/streptomycin and 2 mM glutamine. Lowe cells and control cells were grown in DMEM/F12 (GIBCO BRL) supplemented with 10% fetal bovine serum, ITS supplemented, 4pg/mL triiodothyronine, 36ng/ml dexamethasone, 10ng/ml EGF, 100 U/ml penicillin/streptomycin and 2 mM glutamine at 33°C. For silencing experiments, HeLa cells were transfected with the corresponding siRNA once using HiPerFect (Qiagen) following the manufacturer's instructions. siRNAs were transfected for 72h before imaging. For time-lapse phase contrast microscopy: Transfected cells were plated on 35 mm glass dishes (Iwaki) and put in an open chamber (Life imaging) equilibrated in 5% CO2 and maintained at 37°C. Time-lapse sequences were recorded at 10 min for 60 hr on a Nikon Eclipse Ti Inverted Microscope with a 20x0.45NA plan fluor ELWD objective lens controlled by the Metamorph 6.1 software (Universal Imaging). This microscope was equipped with a cooled CCD camera (HQ2; Ropper Scientific). *m*-3M3FBS (Tocris) or its inactive analog *o*-3M3FBS (Tocris) diluted in DMSO have been added at 25 µM during time-lapse recording.

Zebrafish strains and husbandry

Zebrafish were maintained in standard conditions (Westerfield, 2000) at the University of Manchester Biological Services Unit according to the UK Animals Act 1986. The *ocrl*$^{-/-}$ mutant line (ZDB-GENO-120531–1) has been described previously (Ramirez *et al* 2012). Wild type fish were of AB background.

Lysine-fixable 10 kDa dextran labelled with Alexa 488 (Molecular Probes) was prepared in PBS at 2 µg/µl final concentration. Zebrafish embryos at 72 hpf (hours post fertilisation) were treated for 60 minutes with DMSO control (0.005% DMSO), 5 µM m-3m3fbs or 5 µM o-3m3fbs by addition to the water. Embryos were then anaesthetised with 0.2 mg/ml MS222 (Sigma) in chorion water, and tracer injected into the common cardinal vein using a glass micropipette PLI-90 Pico-Injector (Harvard Apparatus). Embryos were returned to the respective drug treatments and incubated at 29^{o}C. Pronephric accumulation was assessed 2 hours after injection on whole mount embryos using a fluorescent dissecting stereomicroscope (Leica MZ10F). Statistical analysis was performed using the Pearson's chi-squared test with Prism software (Prism Software Corporation).

ACKNOWLEDGMENT: We thank Dr. F. Legendre for generating the patient cell lines described in reference (Dambournet et al., 2011). This work has been supported by CIHR (MOP 133683) and CRSNG découverte to SC laboratory; Institut Pasteur, CNRS, FRM (Equipe FRM DEQ20120323707), ANR (AbCyStem) and the "Association du Syndrome de Lowe" to AE

laboratory. AJC and ML were supported by a research grant from the Lowe Syndrome Trust (ML/MU/2012). K.B.E.K held a doctoral training scholarship from the Fonds de la Recherche du Québec en Santé and was also partially supported by a doctoral scholarships from “La Fondation Desjardins”, from “La Fondation du Grand Défi Pierre Lavoie” and from Montreal University’s molecular biology program. V.E.M held a doctoral scholarship from IRIC and from Montreal University’s molecular biology program.

AUTHOR CONTRIBUTIONS

S.C. managed the project. S.C., V.E.M, K.B.E.K., M.L. and A.E. conceptualized and designed the experiments. V.E.M, K.B.E.K., C.C., A. J-C., E.B. and B.D. performed the experiments. S.C., V.E.M, K.B.E.K., M.L. and A.E. analyzed the data. S.C., V.E.M, K.B.E.K., M.L. and A.E. prepared the figures for the manuscript. S.C., V.E.M and K.B.E.K. wrote the manuscript with input from all coauthors.

FIGURE LEGENDS.

Figure 1. PTEN overexpression prevents cytokinesis and PtdIns(4,5)P_2 homeostasis defects in dOCRL depleted cells, independently of its enzymatic activity.

A. A Schematic depicting the PtdIns pathway. The enzymes in green are the focus of this study. **B.** 4 days after dOCRL dsRNA first treatment, *Drosophila melanogaster* S2 cells were transfected by the indicated GFP tagged constructs. After 2 more days of dOCRL dsRNA treatment and transgene expression, cells were labelled for F-actin (red) and DNA (blue). Asterisks show multinucleated cells. **C.** The graph represents the percentage of multinucleated S2 cells quantified following the indicated treatments; blue dots show individual independent experiments with at least 300 cells/experiment (bars represents mean and SD). P-values (One-way ANOVA) were calculated against the dOCRL dsRNA condition. ns, non-significant ; ****, P < 0.0001. **D.** S2 Cells stably expressing low levels of the PtdIns(4,5)P_2 biosensor, Tubby-GFP, were treated or not (2 bottom rows and top row, respectively) with dOCRL dsRNA. After 4 days of dsRNA treatment, cells were transfected with PTEN$_{C132S}$-mCherry (red) (bottom row). After 2 more days, cells were labelled for DNA (blue) and Tubby-GFP was revealed using an anti-GFP antibody (green). **E.** The ratio of Tubby-GFP fluorescence associated with endomembranes to that associated with the plasma membrane was measured using image J on fixed S2 cells. P-values (Kruskal-Wallis test) were calculated against the non-treated condition. ns, non-significant ; ****, P < 0.0001. N=1, total number of cells >40. Dots represent the ratio for a single cell, bars represents mean and SD.

Figure 2. The PBD and C2 domains of PTEN are necessary and sufficient to prevent the effects of dOCRL depletion.

A. A schematic depicting the five domains of PTEN and the PTEN constructs used in this study. **B.** The graph represents the percentage of multinucleated S2 cells quantified following the indicated treatments; blue dots show individual independent experiment with at least 300 cells/experiment (bars represents mean and SD). Note that multinucleation levels of control and dOCRL-depleted cells was already shown in Figure 1B. P-values (One-way ANOVA) were calculated against the dOCRL dsRNA condition. ns, non-significant ;*, P <0.05; ****, P < 0.0001. **C.** dOCRL dsRNA depleted S2 cells were transfected after 4 days of dsRNA treatment and fixed after 2 days of expression of the indicated GFP tagged PTEN constructs. Cells were labelled for F-actin (red) and DNA (blue). Asterisks show multinucleated cells. **D & E.** The ratio of Tubby-GFP fluorescence associated with endomembranes to that associated with the plasma membrane was measured using image J on fixed S2 cells. P-values (Kruskal-Wallis test) were calculated against the non-treated condition. ns, non-significant ; **, P < 0.01; ****, P < 0.0001. N=1, total number of cells >40 for panel D and >30 for panel E. Dots represent the ratio for a single cell, bars represents mean and SD. Note that the ratio of control and dOCRL-depleted cells was already shown in Figure 1E.

Figure 3. PTEN reduces PtdIns(4,5)P2 levels on endosomes.

A,B,C and G. Two color merged channels is shown in the left row, two-color merged channels of the zoom is shown in the middle row and corresponding BW individual channels is shown in the right row. Note that BW individual channels are displayed in Fig. S3 A, B, C & D. **A.** S2 cells expressing mCh or PTEN$_{PBD-C2}$mCh or PTEN$_{C132S}$mCh (red) were immunostained for Rab7 (green). Arrows show co-localization of the indicated proteins on endosomes. Bar 10 μm. **B.** S2 cells co-expressing mCh or PTEN$_{PBD-C2}$mCh or PTEN$_{C132S}$mCh (red) and GFP-Rab11 (green). Arrows show co-localization of the indicated proteins on endosomes. Bar 10 μm. **C.** S2 cells expressing mCherry (mCh) or PTEN$_{PBD-C2}$mCh or PTEN$_{C132S}$mCh (red) were incubated with LysoTracker Green (green). Arrows show acidic vesicles where PTEN constructs and LysoTracker co-localize. Bar 10 μm. **D.** The ratio of Tubby-GFP fluorescence associated with endomembranes to that associated with the plasma membrane was measured using image J on fixed S2 cells (dots represent the ratio for a single cell, bars represents mean and SD). Green dots represent single cell without Tubby-GFP internal vesicles; Red dots represent single cell with Tubby-GFP internal vesicles. P-values (Mann-Whitney test) were calculated against the non-treated condition for the ratio. ns, non-significant; ***, P < 0.001. N=3, total number of cells >160. **E.** Cells stably expressing low levels of the PtdIns(4,5)P_2 biosensor, Tubby-GFP,

were treated (right) or not (left) with PTEN dsRNA. Bar 10 μm. **F.** Percentage of cells with Tubby-GFP internal vesicles in control and PTEN depleted cells as depicted in D. P-values (one-way Anova) were calculated against the non-treated condition. ns, non-significant; ***, P < 0.001. N=3. total number of cells >160. **G.** S2 cells stably expressing low levels of the PtdIns(4,5)P_2 biosensor, Tubby-GFP (green), were treated with PTEN dsRNA and were incubated with LysoTracker Deep Red (red). Arrows show acidic vesicles positive for the PtdIns(4,5)P_2 biosensor, Tubby-GFP. Bar 10 μm.

Figure 4. A PLC activity is required downstream of PTEN to prevent the effects of dOCRL depletion.

A. Control cells (left row) or dOCRL dsRNA treated S2 cells (2 right rows) were transfected by the $PTEN_{C132S}$-GFP (middle row) or $PTEN_{PBD-C2}$ (left row) after 4 days of dsRNA treatment. Cells were concomitantly treated by 40μm of the PLC inhibitor U-73122. Cells were fixed after 2 days of expression of the transgenes and labelled for F-Actin (red) and DNA (blue). Asterisks show multinucleated cells. **B.** The graph represents the percentage of multinucleated S2 cells quantified following the indicated treatments; blue dots show individual independent experiment with at least 300 cells/experiment (bars represents mean and SD). Note that multinucleation levels of control and dOCRL-depleted cells was already shown in Figure 1B. Each P-values (one-way ANOVA) were calculated using against the dOCRL dsRNA condition *, P < 0.05, **P < 0.01, **** P < 0.0001.

Figure 5. dPLCXD acts downstream of PTEN to compensate for the effects of dOCRL depletion.

A. Cells were treated with the indicated dsRNA. After 4 days, cells were transfected or not (-) with $PTEN_{PBD-C2}$ to assay for dOCRL rescue. Cells were fixed after 2 days and labelled for F-Actin and DNA. The graph represents the percentage of multinucleated S2 cells quantified following the indicated treatments; blue dots show individual independent experiment with at least 300 cells/experiment (bars represents mean and SD). Each P-values (one-way ANOVA) were calculated against the dOCRL dsRNA condition. ns, non-significant; ***, P < 0.001. **B.** Evolutionary tree regrouping PLCXDs from *Drosophila melanogaster*, *Bacillus cereus* and *Homo sapiens* obtained by Multi-way Protein alignment with the scoring matrix BLOSUM 62 on Clone Manager. **C.** Top: domain structure of dPLCXD with the identified "Catalytic domain of phosphoinositide-specific phospholipase C-like phosphodiesterases superfamily" (PI-PLCc_GDPD_SF superfamily, light blue), the X domain (blue green) and the two catalytic histidines (orange). Middle: Conservation of the two catalytic histidines (orange) among *Bacillus cereus* PI-PLC, *Homo sapiens* PLCXD isoforms, and *Drosophila melanogaster* dPLCXD. The last row shows mutations of the two catalytic histidines. Alignment was done by Multi-way Protein alignment with the scoring matrix BLOSUM 62 on Clone Manager. Note that "NCBI conserved domain search" site was used to confirm the two catalytic histidine site of dPLCXD. (https://www.ncbi.nlm.nih.gov/Structure/cdd/wrpsb.cgi). **D.** 2 top rows: S2 cells were transfected with V5 tagged dPLCXD (left) or mutated V5 tagged dPLCXD (HL)2 (right); 2 bottom rows: Cells were treated with dOCRL dsRNA and transfected with V5 tagged dPLCXD (left) or mutated V5 tagged dPLCXD (HL)2 (right). Cells were then labelled for F-Actin (red) and DNA (blue), PLCXD constructs are shown in green. Asterisks show multinucleated cells. Bar 10 μm. **E.** Cells were treated with the dOCRL dsRNA. After 4 days, cells were transfected with dPLCXD or mutated dPLCXD (HL)2. The graph represents the percentage of multinucleated S2 cells quantified following the indicated treatments; blue dots show individual independent experiment with at least 300 cells/experiment (bars represents mean and SD). Each P-values (one-way ANOVA) were calculated against the dOCRL dsRNA condition. ns, non-significant; ****, P < 0.0001.

Figure 6. dPLCXD reduces PtdIns(4,5)P2 levels on endosomes.

A, B and F. Two color merged channels is shown in the left row, two-color merged channels of the zoom is shown in the middle row and corresponding BW individual channels is shown in the right row. Note that BW individual channels are displayed in Fig. S3 E, F & G. **A.** S2 cells expressing dPLCXD-V5 were immunostained for V5 (red) and Rab7 (green). Arrows show co-localization of the indicated proteins on endosomes. Bar 10 μm. **B.** S2 cells co-expressing dPLCXD-V5 and GFP-Rab11 (green) were immunostained for V5 (red). Arrows show co-localization of the indicated proteins on endosomes. Bar 10 μm. **C.** The ratio of Tubby-GFP fluorescence associated with endomembranes to that associated with the plasma membrane was measured using image J on fixed S2 cells (dots represent the ratio for a single cell, bars represents mean and SD). Green dots represent single cell without Tubby-GFP internal vesicles; Red dots represent single cells with Tubby-GFP internal vesicles. P-values (Mann-Whitney test) were calculated against the non-treated condition. ****, $P < 0.0001$. N=3, total number of cells >240. **D.** Cells stably expressing low levels of the PtdIns(4,5)P_2 biosensor, Tubby-GFP, were treated (right) or not (left) with dPLCXD dsRNA. Bar 10 μm. **E.** Percentage of cells with Tubby-GFP internal vesicles in control and dPLCXD depleted cells as depicted in C. P-values (one-way Anova) were calculated against the non-treated condition. ns, non-significant; **, $P < 0.01$. N=3. **F.** S2 cells stably expressing low levels of the PtdIns(4,5)P_2 biosensor, Tubby-GFP (green), were treated with dPLCXD dsRNA and were incubated with LysoTracker Deep Red (red). Arrows show acidic vesicles positive for the PtdIns(4,5)P_2 biosensor, Tubby-GFP. Bar 10 μm.

Figure 7. PTEN acts through dPLCXD to rescue dOCRL depletion.

A. S2 cells co-expressing mCh or $PTEN_{PBD\text{-}C2}$mCh or $PTEN_{C132S}$mCh (red) and dPLCXD-V5, were immunostained for V5 (green). Arrows show vesicles where both indicated proteins localize. Two color merged channels is shown in the left row, two-color merged channels of the zoom is shown in the middle row and corresponding BW individual channels is shown in the right row. Note that BW individual channels are displayed in Fig. S3H. Bar 10 μm. **B.** Cells were treated or not with dOCRL and PTEN dsRNA. After 4 days, cells were transfected with dPLCXD. The graph represents the percentage of multinucleated S2 cells quantified following the indicated treatments; blue dots show individual independent experiment with at least 200 cells/experiment (bars represents mean and SD). Each P-values (one-way ANOVA) were calculated against the control condition. ns, non-significant; ****, $P < 0.0001$. **C.** Representative images used for the histogram in B. Left row: PTEN depleted S2 cells were transfected with V5 tagged dPLCXD or mutated V5 tagged dPLCXD (HL)2 (green); Right row: Cells were treated with PTEN and dOCRL dsRNA and transfected with V5 tagged dPLCXD or mutated V5 tagged dPLCXD (HL)2 (green). Cells were then labelled for F-Actin (red) and DNA (blue). Asterisks show multinucleated cells. Bar 10 μm.

Figure 8. Chemical activation of PLCs prevents dOCRL depletion in Drosophila, dependently of dPLCXD.

A. The ratio of Tubby-GFP fluorescence associated with endomembranes to that associated with the plasma membrane was measured using image J on fixed cells (dots represent the ratio for a single cell, bars represents mean and SD). P-values (Kruskal-Wallis test) were calculated against the non-treated condition. ns, non-significant; ****, $P < 0.0001$. (N=3, total number of cells >190) **B.** Representative images used for the histogram in A. Cells stably expressing low levels of the PtdIns(4,5)P_2 biosensor, Tubby-GFP, were treated for 24 hours with the PLC activator m-3M3FBS or its inactive analog o-3M3FBS both at 25μM. Bar 10 μm. **C.** Control cells (upper panel) or dOCRL dsRNA treated S2 cells (2 bottom panels) were treated for 24 hours with the PLC activator m-3M3FBS or its inactive analog o-3M3FBS both at 25μM. Cells were fixed and labelled for F-Actin (red) and DNA (blue). **D, E and F** The graphs represent the percentage of multinucleated S2 cells quantified following the indicated treatments; blue dots show individual independent experiment with at least 300 cells/experiment (bars represents mean and SD). P-values (One-way ANOVA) were calculated against the non-treated condition. ns, non-significant; *, $P < 0.05$; **, $P < 0.01$; ****, $P < 0.0001$.

Figure 9. Model for regulation of PtdIns(4,5)P_2 homeostasis on endosomes. In Drosophila, PTEN, independently of its enzymatic activity, requires PLCXD to hydrolyze PtdIns(4,5)P_2. This pathway can be chemically activated by m-3M3FBS to compensate for OCRL loss independently of PTEN but dependently on dPLCXD.

Figure 10. Chemical activation of PLC rescues OCRL phenotypes in Lowe syndrome patient cells and a zebrafish Lowe syndrome model. A. Normal renal epithelial cells from a donor not mutated in OCRL and renal epithelial cells from a Lowe syndrome patient were treated with the PLC activator m-3M3FBS or its inactive analog o-3M3FBS. After treatment cell divisions were recorded by time-lapse microscopy. The curves represent the distribution of the abscission times in the indicated cell populations. **B.** Mean abscission times were measured on time-lapse movies in the normal and Lowe renal epithelial cells treated with the PLC activator m-3M3FBS or its inactive analog o-3M3FBS. **C.** Confocal images of pronephric tubules (indicated by a dashed line) in wildtype (WT) and Ocrl-/- zebrafish mutant embryos. The indicated embryos were injected with Alexa 488-10 kDa dextran (green) and treated with the PLC activator m-3M3FBS or its inactive analog o-3M3FBS. **D.** Pronephric accumulation in the indicated embryos was monitored by fluorescence microscopy. ns, non-significant; *, $P < 0.05$; **, $P < 0.01$; ***, $P < 0.001$; ****, $P < 0.0001$ (Pearson's chi-squared test). Bar 10 μm.

Figure S1. A balance of Skittles and dOCRL activities regulates PtdIns(4,5)P_2 on endomembranes and cytokinesis outcome.

A. S2 cells were transiently transfected with Skittles-GFP, fixed and labelled for F-Actin (red) and DNA (blue). Note that Skittles expression triggers endosome enlargement. Bar 10 μm. **B.** dOCRL depleted S2 cells were transiently transfected with Skittles-GFP, fixed and labelled for F-Actin (red) and DNA (blue). Note that Skittles expression triggers endosome enlargement. Bar 10 μm. **C, D and E** The graphs represent the percentage of multinucleated S2 cells quantified following the indicated treatments; blue dots show individual independent experiment with at least 300 cells/experiment (bars represents mean and SD). P-values (One-way ANOVA) were calculated against the non-treated condition. ns, non-significant; ****, $P < 0.0001$.

Figure S2. The PBD and C2 domains of PTEN are necessary to rescue dOCRL depletion. A. dOCRL dsRNA treated cells were transfected by the indicated cDNA after 4 days of dsRNA treatment and fixed 2 days after. Cells were labelled for F-actin (red) and DNA (blue). Asterisks show multinucleated cells. Bar 10 μm. **B.** Western Blot on cell extract transiently transfected by the PTEN constructs used in Figure 1 and 2. The chimera were revealed using a α-GFP antibody. Note that some chimeras are cleaved and the Western blot revealed cleaved GFP.

F**igure S3. PTEN, dPLCXD and the PtdIns(4,5)P2 biosensor Tubby-GFP co-localize with endosome markers.**

A. S2 cells expressing $PTEN_{PBD\text{-}C2}$mCh or $PTEN_{C132S}$mCh (red) were immunostained for Rab7 (green). Arrows show co-localization of the indicated proteins on endosomes. Bar 10 μm. **B.** S2 cells co-expressing $PTEN_{PBD\text{-}C2}$mCh or $PTEN_{C132S}$mCh (red) and GFP-Rab11 (green). Arrows show co-localization of the indicated proteins on endosomes. Bar 10 μm. **C.** S2 cells expressing $PTEN_{PBD\text{-}C2}$mCh or $PTEN_{C132S}$mCh (red) were incubated with LysoTracker Green (green). Arrows show acidic vesicles where PTEN constructs and LysoTracker co-localize. Bar 10 μm. **D.** S2 cells stably expressing low levels of the PtdIns(4,5)P_2 biosensor, Tubby-GFP (green), were treated with PTEN dsRNA and were incubated with LysoTracker Deep Red (red). Arrows show acidic vesicles positive for the PtdIns(4,5)P_2 biosensor, Tubby-GFP. Bar 10 μm. **E.** S2 cells expressing dPLCXD-V5 were immunostained for V5 (red) and Rab7

(green). Arrows show co-localization of the indicated proteins on endosomes. Bar 10 μm. **F.** S2 cells co-expressing dPLCXD-V5 and GFP-Rab11 (green) were immunostained for V5 (red). Arrows show co-localization of the indicated proteins on endosomes. Bar 10 μm. **G.** S2 cells stably expressing low levels of the PtdIns(4,5)P_2 biosensor, Tubby-GFP (green), were treated with dPLCXD dsRNA and were incubated with LysoTracker Deep Red (red). Arrows show acidic vesicles positive for the PtdIns(4,5)P_2 biosensor, Tubby-GFP. Bar 10 μm. **H.** S2 cells co-expressing $PTEN_{PBD\text{-}C2}$mCh or $PTEN_{C132S}$mCh (red) and dPLCXD-V5, were immunostained for V5 (green). Arrows show vesicles where both indicated proteins localize. Bar 10 μm.

Figure S4. Depletion of other PLCs than dPLCXD does not affect PTEN rescue of dOCRL depletion.

A. The graph represents the percentage of multinucleated S2 cells quantified following the indicated treatments; blue diamonds show the percentage of individual independent experiments with n>300 cells (bars represents mean and SD). P-values (t-test) were calculated against the non-treated condition. ns, non-significant. **B.** The graph represents the percentage of multinucleated cells quantified following the indicated treatments; blue diamonds show the percentage of individual independents experiments, n>300 cells (bars represents mean and SD). Each P-values (one-way ANOVA) were calculated against the dOCRL dsRNA condition. ns, non-significant; **, $P < 0.01$, ***, $P < 0.001$. **C.** The graph represents the percentage of multinucleated S2 cells quantified following the indicated treatments; blue diamonds show the percentage of individual independent experiments with n>300 cells (bars represents mean and SD). P-values (t-test) were calculated against the non-treated condition. ns, non-significant.

Figure S5. Chemical activation of PLC rescues delayed abscission in HeLa cells treated with OCRL RNai. A. DMSO (Vehicle), the PLC activator m-3M3FBS or its inactive analog o-3M3FBS was added to HeLa cells treated with the indicated RNAi. Cell divisions were recorded by time-lapse microscopy. The curves represent the distribution of the abscission times in the indicated cell populations. **B.** Mean abscission times were measured on time-lapse movies quantified in A. ns, non-significant; **, $P < 0.01$, ***, $P < 0.001$.

REFERENCES

BAE, Y. S., LEE, T. G., PARK, J. C., HUR, J. H., KIM, Y., HEO, K., KWAK, J. Y., SUH, P. G. & RYU, S. H. 2003. Identification of a compound that directly stimulates phospholipase C activity. *Mol Pharmacol,* 63**,** 1043-50.

BALLA, T. 2013. Phosphoinositides: tiny lipids with giant impact on cell regulation. *Physiol Rev,* 93**,** 1019-137.

BEN EL KADHI, K., EMERY, G. & CARRENO, S. 2012. The unexpected role of Drosophila OCRL during cytokinesis. *Commun Integr Biol,* 5**,** 291-3.

BEN EL KADHI, K., ROUBINET, C., SOLINET, S., EMERY, G. & CARRENO, S. 2011. The Inositol 5-Phosphatase dOCRL Controls PI(4,5)P2 Homeostasis and Is Necessary for Cytokinesis. *Current biology : CB,* 21**,** 1074-9.

BENES, C. H., WU, N., ELIA, A. E., DHARIA, T., CANTLEY, L. C. & SOLTOFF, S. P. 2005. The C2 domain of PKCdelta is a phosphotyrosine binding domain. *Cell,* 121**,** 271-80.

BOCKENHAUER, D., BOKENKAMP, A., VAN'T HOFF, W., LEVTCHENKO, E., KIST-VAN HOLTHE, J. E., TASIC, V. & LUDWIG, M. 2008. Renal phenotype in Lowe Syndrome: a selective proximal tubular dysfunction. *Clin J Am Soc Nephrol,* 3**,** 1430-6.

BOKENKAMP, A., BOCKENHAUER, D., CHEONG, H. I., HOPPE, B., TASIC, V., UNWIN, R. & LUDWIG, M. 2009. Dent-2 disease: a mild variant of Lowe syndrome. *J Pediatr,* 155**,** 94-9.

CARIM, S. C., BEN EL KADHI, K., YAN, G., SWEENEY, S. T., HICKSON, G. R., CARRENO, S. & LOWE, M. 2019. IPIP27 Coordinates PtdIns(4,5)P2 Homeostasis for Successful Cytokinesis. *Curr Biol,* 29**,** 775-789 e7.

CAUVIN, C. & ECHARD, A. 2015. Phosphoinositides: Lipids with informative heads and mastermind functions in cell division. *Biochim Biophys Acta,* 1851**,** 832-43.

CAUVIN, C., ROSENDALE, M., GUPTA-ROSSI, N., ROCANCOURT, M., LARRAUFIE, P., SALOMON, R., PERRAIS, D. & ECHARD, A. 2016. Rab35 GTPase Triggers Switch-like Recruitment of the Lowe Syndrome Lipid Phosphatase OCRL on Newborn Endosomes. *Curr Biol,* 26**,** 120-8.

CHOUDHURY, R., DIAO, A., ZHANG, F., EISENBERG, E., SAINT-POL, A., WILLIAMS, C., KONSTANTAKOPOULOS, A., LUCOCQ, J., JOHANNES, L., RABOUILLE, C., GREENE, L. E. & LOWE, M. 2005. Lowe syndrome protein OCRL1 interacts with clathrin and regulates protein trafficking between endosomes and the trans-Golgi network. *Molecular biology of the cell,* 16**,** 3467-79.

CORBALAN-GARCIA, S. & GOMEZ-FERNANDEZ, J. C. 2014. Signaling through C2 domains: more than one lipid target. *Biochim Biophys Acta,* 1838**,** 1536-47.

DAMBOURNET, D., MACHICOANE, M., CHESNEAU, L., SACHSE, M., ROCANCOURT, M., EL MARJOU, A., FORMSTECHER, E., SALOMON, R., GOUD, B. & ECHARD, A. 2011. Rab35 GTPase and OCRL phosphatase remodel lipids and F-actin for successful cytokinesis. *Nat Cell Biol,* 13**,** 981-8.

DE LEO, M. G., STAIANO, L., VICINANZA, M., LUCIANI, A., CARISSIMO, A., MUTARELLI, M., DI CAMPLI, A., POLISHCHUK, E., DI TULLIO, G., MORRA, V., LEVTCHENKO, E., OLTRABELLA, F., STARBORG, T., SANTORO, M., DI BERNARDO, D., DEVUYST, O., LOWE, M., MEDINA, D. L., BALLABIO, A. & DE MATTEIS, M. A. 2016. Autophagosome-lysosome fusion triggers a lysosomal response mediated by TLR9 and controlled by OCRL. *Nat Cell Biol,* 18**,** 839-50.

DE MATTEIS, M. A., STAIANO, L., EMMA, F. & DEVUYST, O. 2017. The 5-phosphatase OCRL in Lowe syndrome and Dent disease 2. *Nat Rev Nephrol,* 13**,** 455-470.

DEL SIGNORE, S. J., BIBER, S. A., LEHMANN, K. S., HEIMLER, S. R., ROSENFELD, B. H., ESKIN, T. L., SWEENEY, S. T. & RODAL, A. A. 2017. dOCRL maintains immune cell quiescence by regulating endosomal traffic. *PLoS Genet,* 13**,** e1007052.

EMOTO, K., INADOME, H., KANAHO, Y., NARUMIYA, S. & UMEDA, M. 2005. Local change in phospholipid composition at the cleavage furrow is essential for completion of cytokinesis. *J Biol Chem,* 280**,** 37901-7.

ERDMANN, K. S., MAO, Y., MCCREA, H. J., ZONCU, R., LEE, S., PARADISE, S., MODREGGER, J., BIEMESDERFER, D., TOOMRE, D. & DE CAMILLI, P. 2007. A role of the Lowe syndrome protein OCRL in early steps of the endocytic pathway. *Dev Cell,* 13**,** 377-90.

ESSEN, L. O., PERISIC, O., KATAN, M., WU, Y., ROBERTS, M. F. & WILLIAMS, R. L. 1997. Structural mapping of the catalytic mechanism for a mammalian phosphoinositide-specific phospholipase C. *Biochemistry,* 36**,** 1704-18.

FIELD, S. J., MADSON, N., KERR, M. L., GALBRAITH, K. A., KENNEDY, C. E., TAHILIANI, M., WILKINS, A. & CANTLEY, L. C. 2005. PtdIns(4,5)P2 functions at the cleavage furrow during cytokinesis. *Curr Biol,* 15**,** 1407-12.

GELLATLY, S. A., KALUJNAIA, S. & CRAMB, G. 2012. Cloning, tissue distribution and sub-cellular localisation of phospholipase C X-domain containing protein (PLCXD) isoforms. *Biochem Biophys Res Commun,* 424**,** 651-6.

HEINZ, D. W., RYAN, M., BULLOCK, T. L. & GRIFFITH, O. H. 1995. Crystal structure of the phosphatidylinositol-specific phospholipase C from Bacillus cereus in complex with myo-inositol. *EMBO J,* 14**,** 3855-63.

ILMONEN, S., VAHERI, A., ASKO-SELJAVAARA, S. & CARPEN, O. 2005. Ezrin in primary cutaneous melanoma. *Mod Pathol,* 18**,** 503-10.

KADAMUR, G. & ROSS, E. M. 2013. Mammalian phospholipase C. *Annu Rev Physiol,* 75**,** 127-54.

KIM, S. D., KIM, H. J., SHIM, J. W., LEE, H. Y., LEE, S. K., KWON, S., JUNG, Y. S., BAEK, S. H., PARK, J. S., ZABEL, B. A. & BAE, Y. S. 2012. Phospholipase C activator m-3M3FBS protects against morbidity and mortality associated with sepsis. *J Immunol,* 189**,** 2000-5.

KOLAY, S., BASU, U. & RAGHU, P. 2016. Control of diverse subcellular processes by a single multi-functional lipid phosphatidylinositol 4,5-bisphosphate [PI(4,5)P2]. *Biochem J,* 473**,** 1681-92.

LI, C., ULLRICH, B., ZHANG, J. Z., ANDERSON, R. G., BROSE, N. & SUDHOF, T. C. 1995. Ca(2+)-dependent and -independent activities of neural and non-neural synaptotagmins. *Nature,* 375**,** 594-9.

LIU, J., FAIRN, G. D., CECCARELLI, D. F., SICHERI, F. & WILDE, A. 2012. Cleavage furrow organization requires PIP(2)-mediated recruitment of anillin. *Curr Biol,* 22**,** 64-9.

MAEHAMA, T. & DIXON, J. E. 1998. The tumor suppressor, PTEN/MMAC1, dephosphorylates the lipid second messenger, phosphatidylinositol 3,4,5-trisphosphate. *J Biol Chem,* 273**,** 13375-8.

MAJZOUB, R. N., WONDER, E., EWERT, K. K., KOTAMRAJU, V. R., TEESALU, T. & SAFINYA, C. R. 2016. Rab11 and Lysotracker Markers Reveal Correlation between Endosomal Pathways and Transfection Efficiency of Surface-Functionalized Cationic Liposome-DNA Nanoparticles. *J Phys Chem B,* 120**,** 6439-53.

MEHTA, Z. B., PIETKA, G. & LOWE, M. 2014. The cellular and physiological functions of the Lowe syndrome protein OCRL1. *Traffic,* 15**,** 471-87.

NAGUIB, A., BENCZE, G., CHO, H., ZHENG, W., TOCILJ, A., ELKAYAM, E., FAEHNLE, C. R., JABER, N., PRATT, C. P., CHEN, M., ZONG, W. X., MARKS, M. S., JOSHUA-TOR, L., PAPPIN, D. J. & TROTMAN, L. C. 2015. PTEN functions by recruitment to cytoplasmic vesicles. *Mol Cell,* 58**,** 255-68.

NANDEZ, R., BALKIN, D. M., MESSA, M., LIANG, L., PARADISE, S., CZAPLA, H., HEIN, M. Y., DUNCAN, J. S., MANN, M. & DE CAMILLI, P. 2014. A role of OCRL in clathrin-coated pit dynamics and uncoating revealed by studies of Lowe syndrome cells. *Elife,* 3**,** e02975.

OLTRABELLA, F., PIETKA, G., RAMIREZ, I. B., MIRONOV, A., STARBORG, T., DRUMMOND, I. A., HINCHLIFFE, K. A. & LOWE, M. 2015. The Lowe syndrome protein OCRL1 is required for endocytosis in the zebrafish pronephric tubule. *PLoS Genet,* 11**,** e1005058.

PIRRUCCELLO, M. & DE CAMILLI, P. 2012. Inositol 5-phosphatases: insights from the Lowe syndrome protein OCRL. *Trends in Biochemical Sciences,* 37**,** 134-143.

QUINN, K. V., BEHE, P. & TINKER, A. 2008. Monitoring changes in membrane phosphatidylinositol 4,5-bisphosphate in living cells using a domain from the transcription factor tubby. *J Physiol,* 586**,** 2855-71.

RAFTOPOULOU, M., ETIENNE-MANNEVILLE, S., SELF, A., NICHOLLS, S. & HALL, A. 2004. Regulation of cell migration by the C2 domain of the tumor suppressor PTEN. *Science,* 303**,** 1179-81.

RAMIREZ, I. B., PIETKA, G., JONES, D. R., DIVECHA, N., ALIA, A., BARABAN, S. C., HURLSTONE, A. F. & LOWE, M. 2012. Impaired neural development in a zebrafish model for Lowe syndrome. *Hum Mol Genet,* 21**,** 1744-59.

ROUBINET, C., DECELLE, B., CHICANNE, G., DORN, J. F., PAYRASTRE, B., PAYRE, F. & CARRENO, S. 2011. Molecular networks linked by Moesin drive remodeling of the cell cortex during mitosis. *J Cell Biol,* 195**,** 99-112.

SHINDE, S. R. & MADDIKA, S. 2016. PTEN modulates EGFR late endocytic trafficking and degradation by dephosphorylating Rab7. *Nat Commun,* 7**,** 10689.

SMITH, R. J., SAM, L. M., JUSTEN, J. M., BUNDY, G. L., BALA, G. A. & BLEASDALE, J. E. 1990. Receptor-coupled signal transduction in human polymorphonuclear neutrophils: effects of a novel inhibitor of phospholipase C-dependent processes on cell responsiveness. *J Pharmacol Exp Ther,* 253**,** 688-97.

SONG, M. S., SALMENA, L. & PANDOLFI, P. P. 2012. The functions and regulation of the PTEN tumour suppressor. *Nat Rev Mol Cell Biol,* 13**,** 283-96.

SZENTPETERY, Z., BALLA, A., KIM, Y. J., LEMMON, M. A. & BALLA, T. 2009. Live cell imaging with protein domains capable of recognizing phosphatidylinositol 4,5-bisphosphate; a comparative study. *BMC Cell Biol,* 10**,** 67.

UNGEWICKELL, A., WARD, M. E., UNGEWICKELL, E. & MAJERUS, P. W. 2004. The inositol polyphosphate 5-phosphatase Ocrl associates with endosomes that are partially coated with clathrin. *Proceedings of the National Academy of Sciences of the United States of America,* 101**,** 13501-6.

VIAUD, J., MANSOUR, R., ANTKOWIAK, A., MUJALLI, A., VALET, C., CHICANNE, G., XUEREB, J. M., TERRISSE, A. D., SEVERIN, S., GRATACAP, M. P., GAITS-IACOVONI, F. & PAYRASTRE, B. 2016. Phosphoinositides: Important lipids in the coordination of cell dynamics. *Biochimie,* 125**,** 250-8.

VICINANZA, M., DI CAMPLI, A., POLISHCHUK, E., SANTORO, M., DI TULLIO, G., GODI, A., LEVTCHENKO, E., DE LEO, M. G., POLISHCHUK, R., SANDOVAL, L., MARZOLO, M. & DE MATTEIS, M. A. 2011. OCRL controls trafficking through early endosomes via PtdIns4,5P(2)-dependent regulation of endosomal actin. *EMBO J*.

WORBY, C. A. & DIXON, J. E. 2014. Pten. *Annu Rev Biochem,* 83**,** 641-69.

YOSHIDA, A., HAYASHI, H., TANABE, K. & FUJITA, A. 2017. Segregation of phosphatidylinositol 4-phosphate and phosphatidylinositol 4,5-bisphosphate into distinct microdomains on the endosome membrane. *Biochim Biophys Acta Biomembr,* 1859**,** 1880-1890.

Figure 1

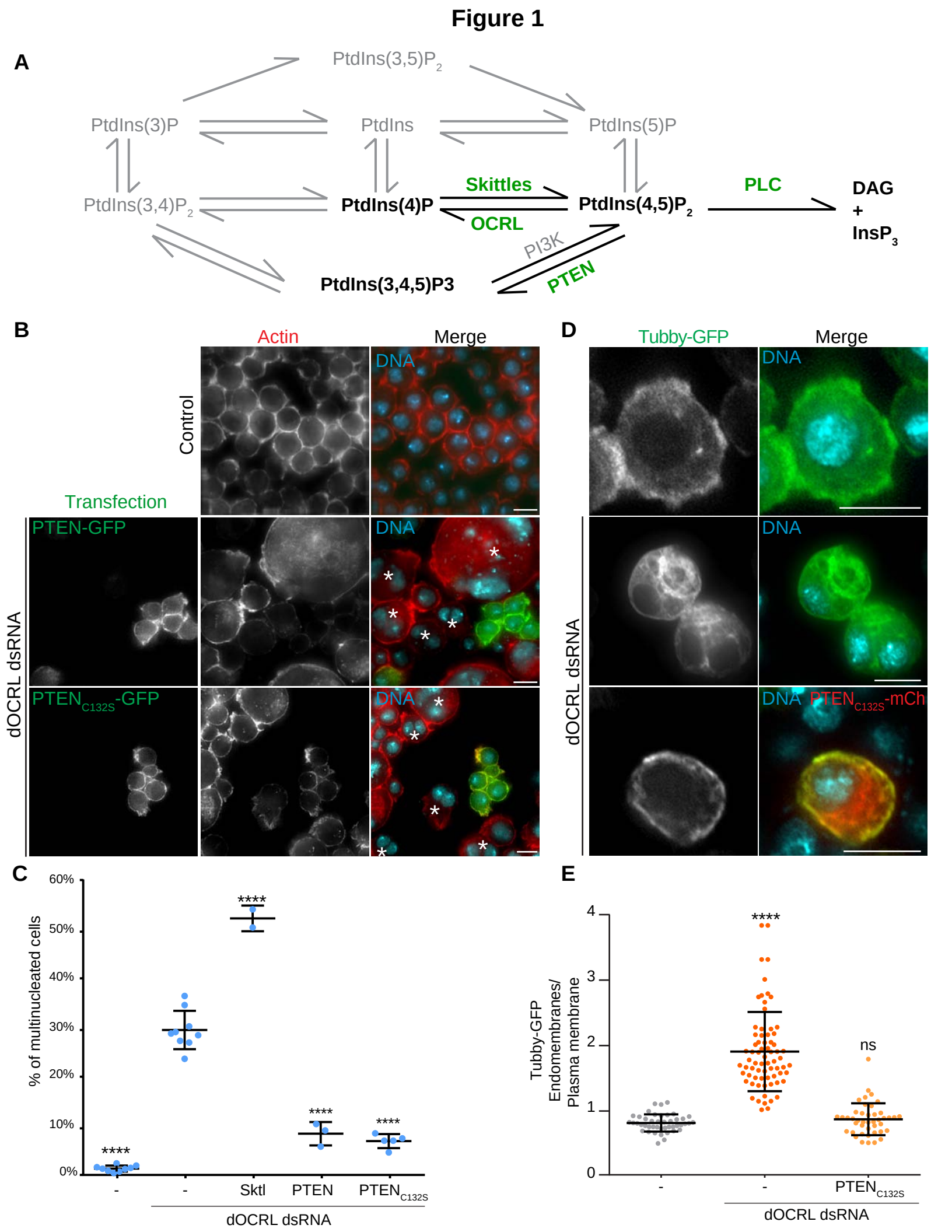
A
PtdIns(3,5)P2
PtdIns(3)P
PtdIns
PtdIns(5)P
PtdIns(3,4)P2
PtdIns(4)P
Skittles
OCRL
PtdIns(4,5)P2
PLC
DAG
+
InsP3
PI3K
PTEN
PtdIns(3,4,5)P3
B
Actin
Merge
Control
DNA
Transfection
PTEN-GFP
dOCRL dsRNA
PTENC132S-GFP
D
Tubby-GFP
Merge
DNA
dOCRL dsRNA
PTENC132S-mCh
C
% of multinucleated cells
60%
50%
40%
30%
20%
10%
0%
****
-
Sktl
PTEN
PTENC132S
dOCRL dsRNA
E
Tubby-GFP
Endomembranes/
Plasma membrane
4
3
2
1
0
ns

Figure 2

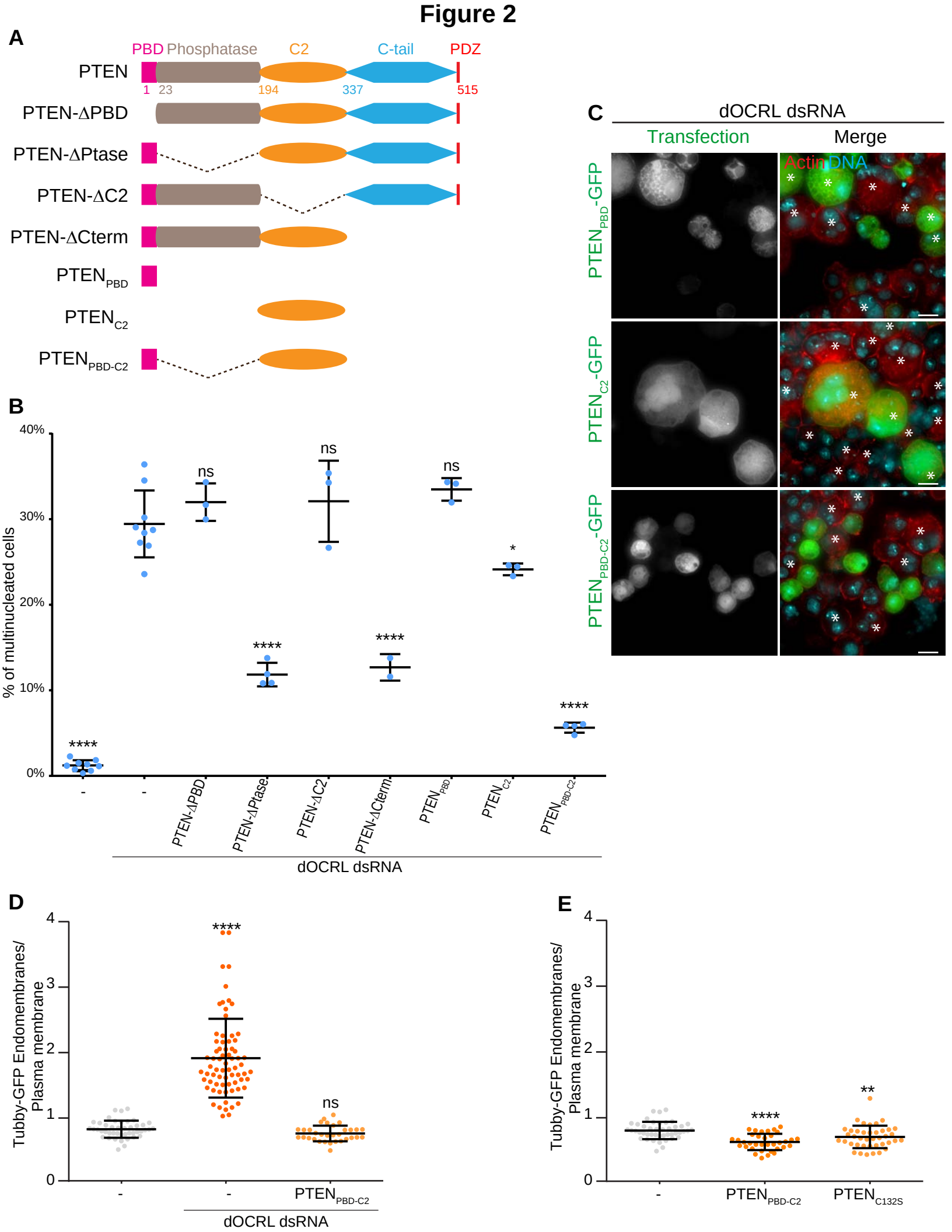
A
PBD
Phosphatase
C2
C-tail
PDZ
PTEN
1
23
194
337
515
PTEN-ΔPBD
PTEN-ΔPtase
PTEN-ΔC2
PTEN-ΔCterm
PTEN PBD
PTEN C2
PTEN PBD-C2
B
% of multinucleated cells
40%
30%
20%
10%
0%
ns
****
*
-
PTEN-ΔPBD
PTEN-ΔPtase
PTEN-ΔC2
PTEN-ΔCterm
PTEN PBD
PTEN C2
PTEN PBD-C2
dOCRL dsRNA
C
dOCRL dsRNA
Transfection
Merge
Actin DNA
PTEN PBD-GFP
PTEN C2-GFP
PTEN PBD-C2-GFP
D
Tubby-GFP Endomembranes/ Plasma membrane
4
3
2
1
0
****
ns
-
PTEN PBD-C2
dOCRL dsRNA
E
Tubby-GFP Endomembranes/ Plasma membrane
4
3
2
1
0
****
**
-
PTEN PBD-C2
PTEN C132S

Figure 3

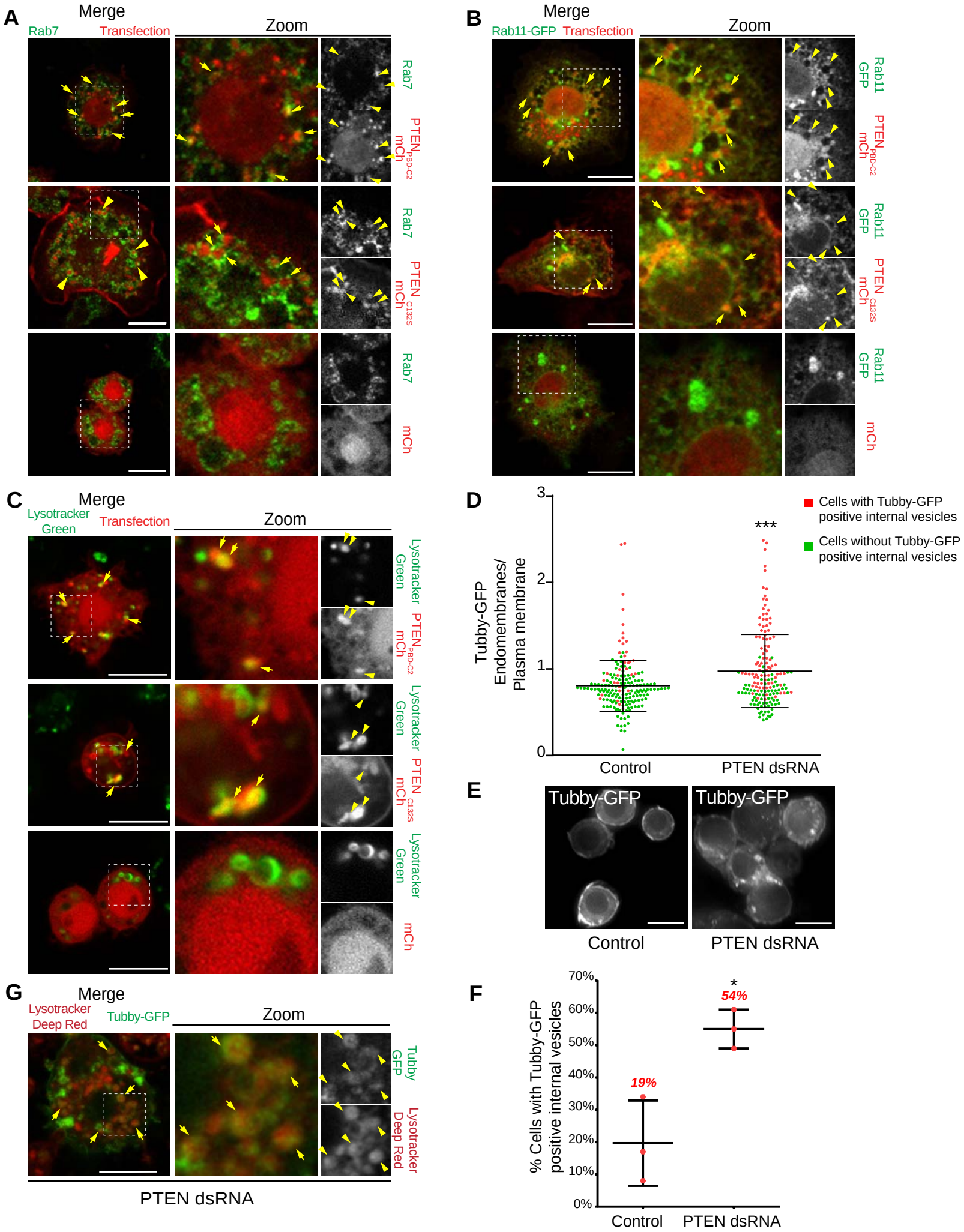
A
Merge
Rab7
Transfection
Zoom
Rab7
PTEN PBD-C2 mCh
Rab7
PTEN C132S mCh
Rab7
mCh
B
Merge
Rab11-GFP
Transfection
Zoom
Rab11 GFP
PTEN PBD-C2 mCh
Rab11 GFP
PTEN C132S mCh
Rab11 GFP
mCh
C
Merge
Lysotracker Green
Transfection
Zoom
Lysotracker Green
PTEN PBD-C2 mCh
Lysotracker Green
PTEN C132S mCh
Lysotracker Green
mCh
D
Tubby-GFP Endomembranes/ Plasma membrane
Cells with Tubby-GFP positive internal vesicles
Cells without Tubby-GFP positive internal vesicles
***
Control
PTEN dsRNA
E
Tubby-GFP
Tubby-GFP
Control
PTEN dsRNA
F
% Cells with Tubby-GFP positive internal vesicles
19%
*
54%
Control
PTEN dsRNA
G
Merge
Lysotracker Deep Red
Tubby-GFP
Zoom
Tubby GFP
Lysotracker Deep Red
PTEN dsRNA

Figure 4

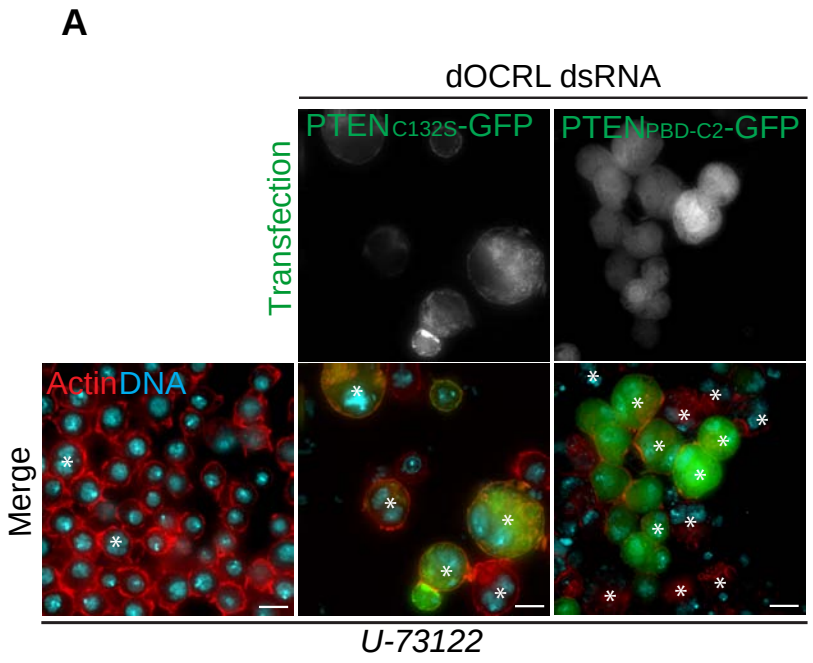
A
dOCRL dsRNA
Transfection
PTENC132S-GFP
PTENPBD-C2-GFP
Actin DNA
Merge
U-73122

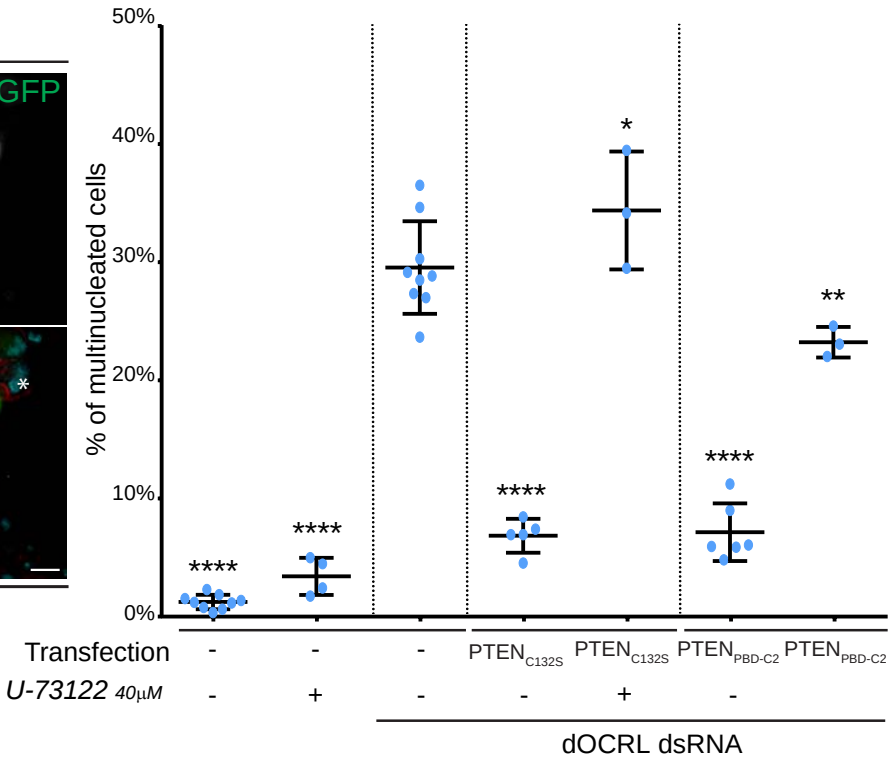
B
% of multinucleated cells
50%
40%
30%
20%
10%
0%
****
****
****
*
****
**
Transfection
PTENC132S
PTENC132S
PTENPBD-C2
PTENPBD-C2
U-73122 40μM
dOCRL dsRNA

Figure 5

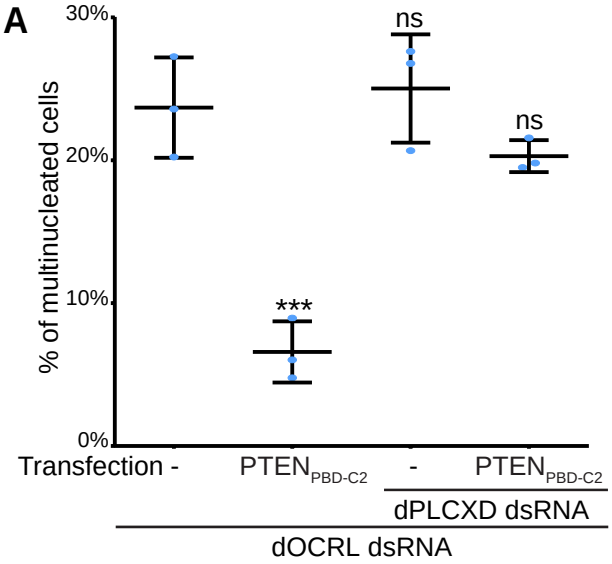
A
30%
20%
10%
0%
% of multinucleated cells
ns
ns
***
Transfection -
PTEN PBD-C2
-
PTEN PBD-C2
dPLCXD dsRNA
dOCRL dsRNA

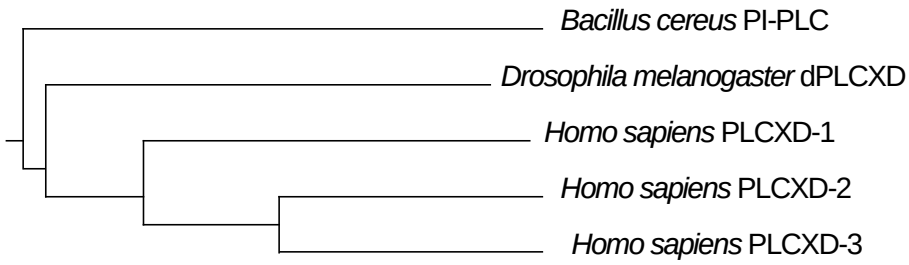
B
Bacillus cereus PI-PLC
Drosophila melanogaster dPLCXD
Homo sapiens PLCXD-1
Homo sapiens PLCXD-2
Homo sapiens PLCXD-3

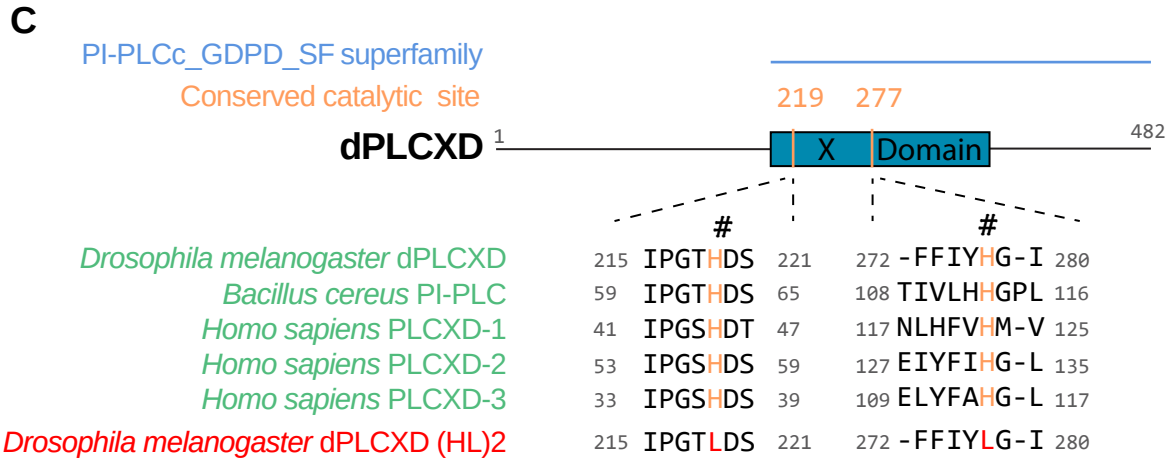
C
PI-PLCc_GDPD_SF superfamily
Conserved catalytic site
219
277
dPLCXD
1
X
Domain
482
#
#
Drosophila melanogaster dPLCXD 215 IPGTHDS 221 272 -FFIYHG-I 280
Bacillus cereus PI-PLC 59 IPGTHDS 65 108 TIVLHHGPL 116
Homo sapiens PLCXD-1 41 IPGSHDT 47 117 NLHFVHM-V 125
Homo sapiens PLCXD-2 53 IPGSHDS 59 127 EIYFIHG-L 135
Homo sapiens PLCXD-3 33 IPGSHDS 39 109 ELYFAHG-L 117
Drosophila melanogaster dPLCXD (HL)2 215 IPGTLDS 221 272 -FFIYLG-I 280

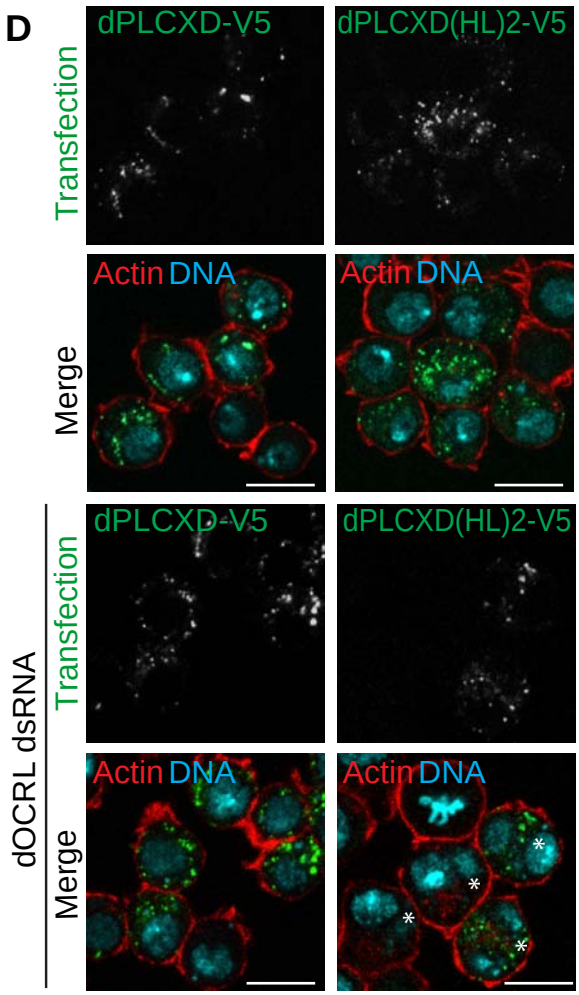
D
dPLCXD-V5
dPLCXD(HL)2-V5
Transfection
Actin DNA
Actin DNA
Merge
dPLCXD-V5
dPLCXD(HL)2-V5
Transfection
dOCRL dsRNA
Actin DNA
Actin DNA
Merge

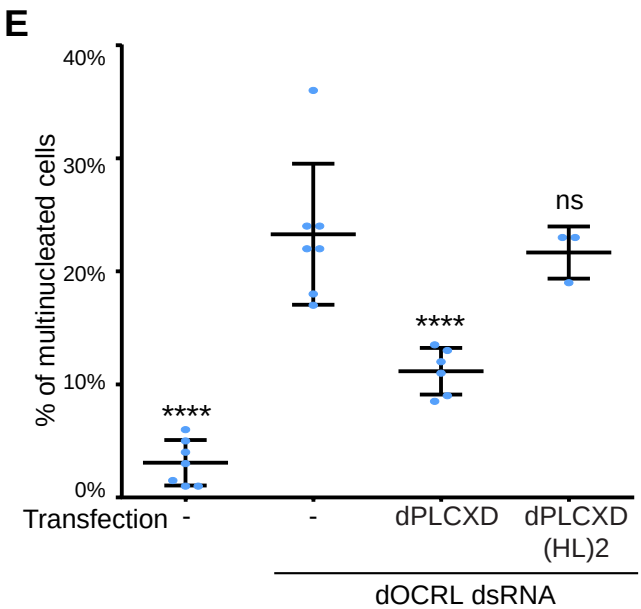
E
40%
30%
20%
10%
0%
% of multinucleated cells
****
****
ns
Transfection -
-
dPLCXD
dPLCXD (HL)2
dOCRL dsRNA

Figure 6

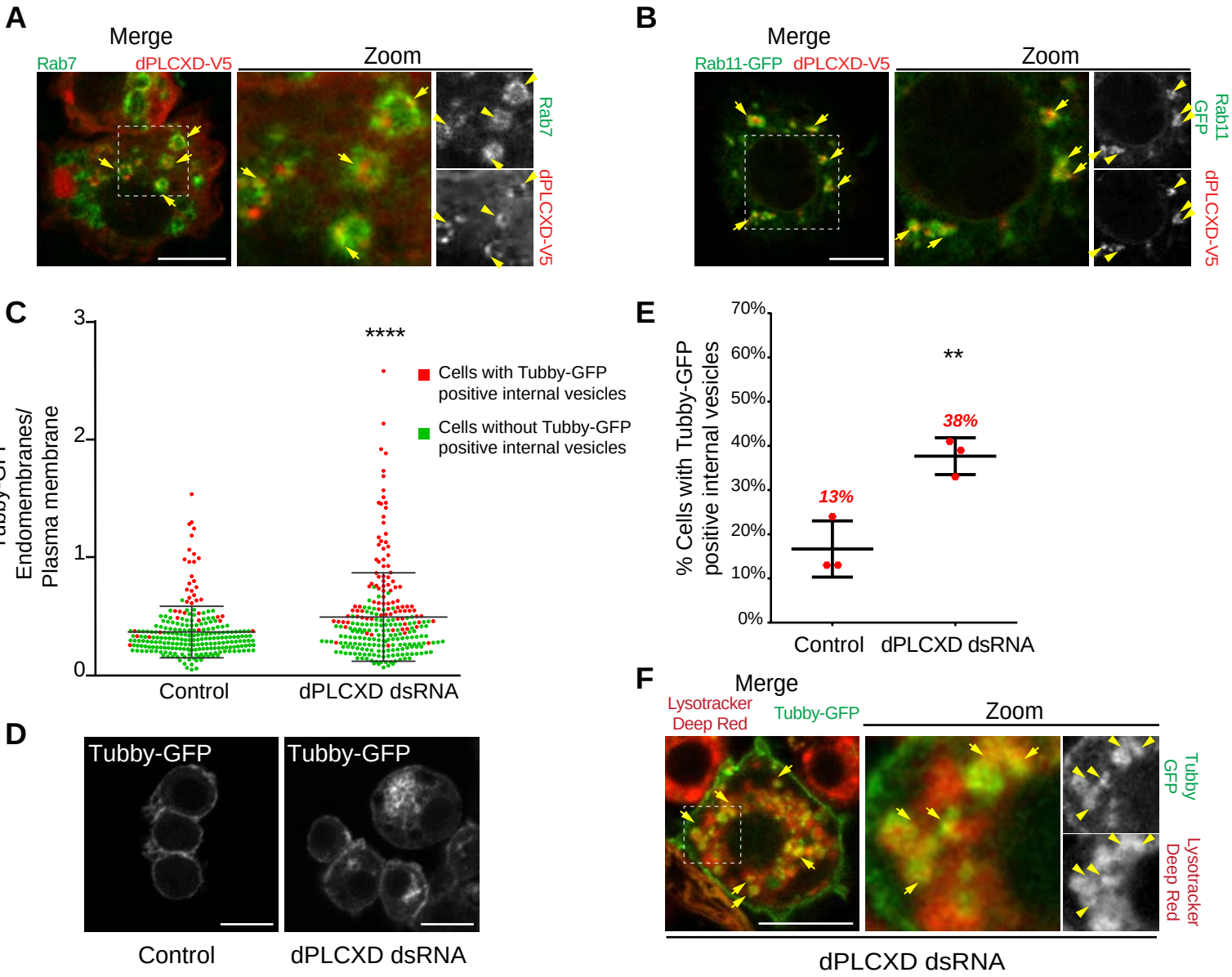
A
Merge
Rab7
dPLCXD-V5
Zoom
Rab7
dPLCXD-V5
B
Merge
Rab11-GFP
dPLCXD-V5
Zoom
Rab11 GFP
dPLCXD-V5
C
Tubby-GFP Endomembranes/ Plasma membrane
3
2
1
0
****
Cells with Tubby-GFP positive internal vesicles
Cells without Tubby-GFP positive internal vesicles
Control
dPLCXD dsRNA
D
Tubby-GFP
Tubby-GFP
Control
dPLCXD dsRNA
E
% Cells with Tubby-GFP positive internal vesicles
70%
60%
50%
40%
30%
20%
10%
0%
**
38%
13%
Control
dPLCXD dsRNA
F
Merge
Lysotracker Deep Red
Tubby-GFP
Zoom
Tubby GFP
Lysotracker Deep Red
dPLCXD dsRNA

Figure 7

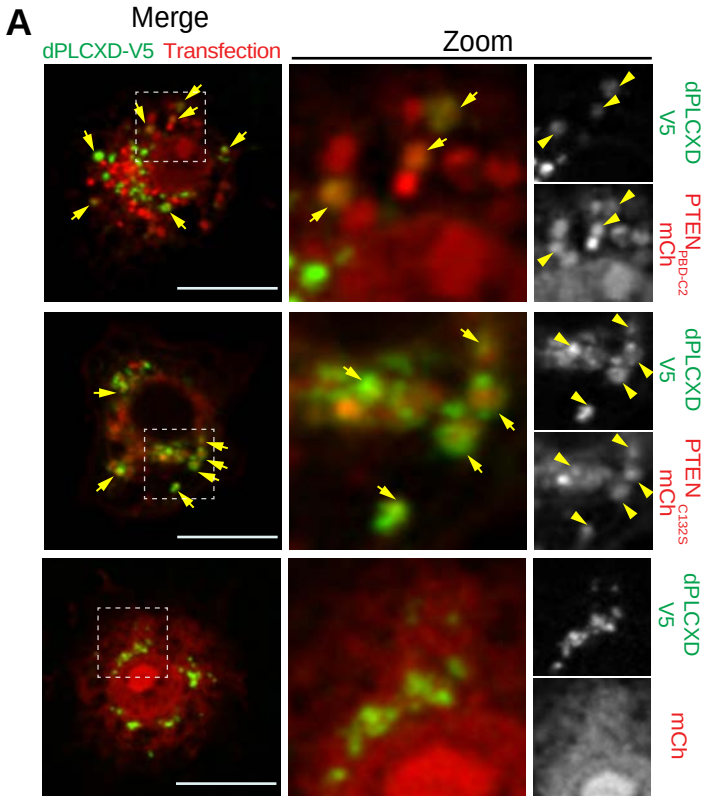
A
Merge
dPLCXD-V5 Transfection
Zoom
dPLCXD V5
PTEN PBD-C2 mCh
dPLCXD V5
PTEN C132S mCh
dPLCXD V5
mCh

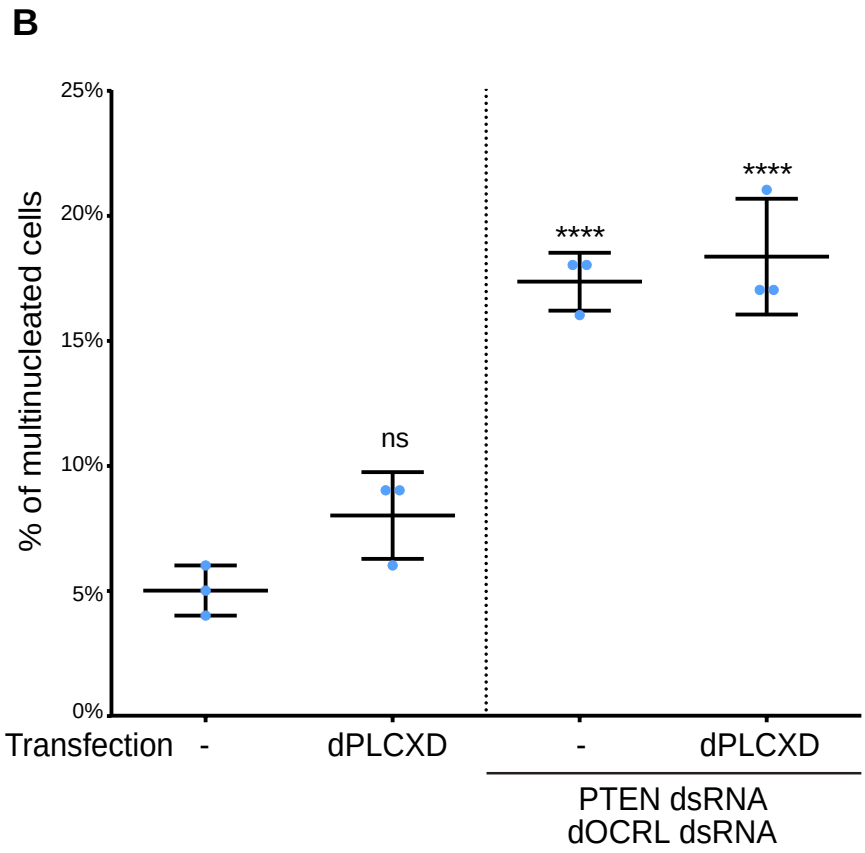
B
% of multinucleated cells
25%
20%
15%
10%
5%
0%
ns
****
****
Transfection
-
dPLCXD
-
dPLCXD
PTEN dsRNA
dOCRL dsRNA

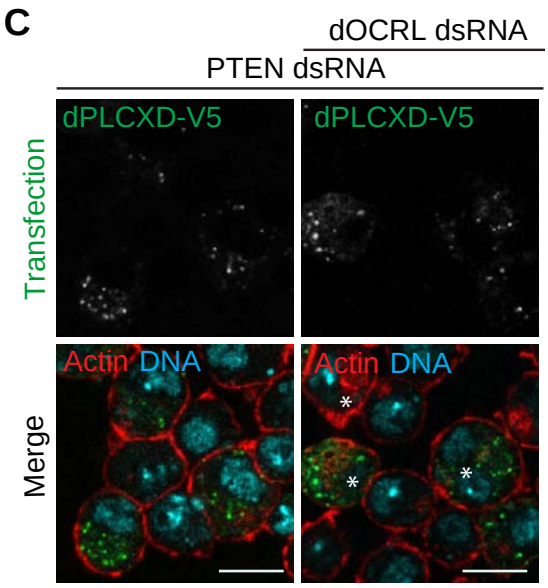
C
dOCRL dsRNA
PTEN dsRNA
Transfection
Merge
dPLCXD-V5
dPLCXD-V5
Actin DNA
Actin DNA

Figure 8

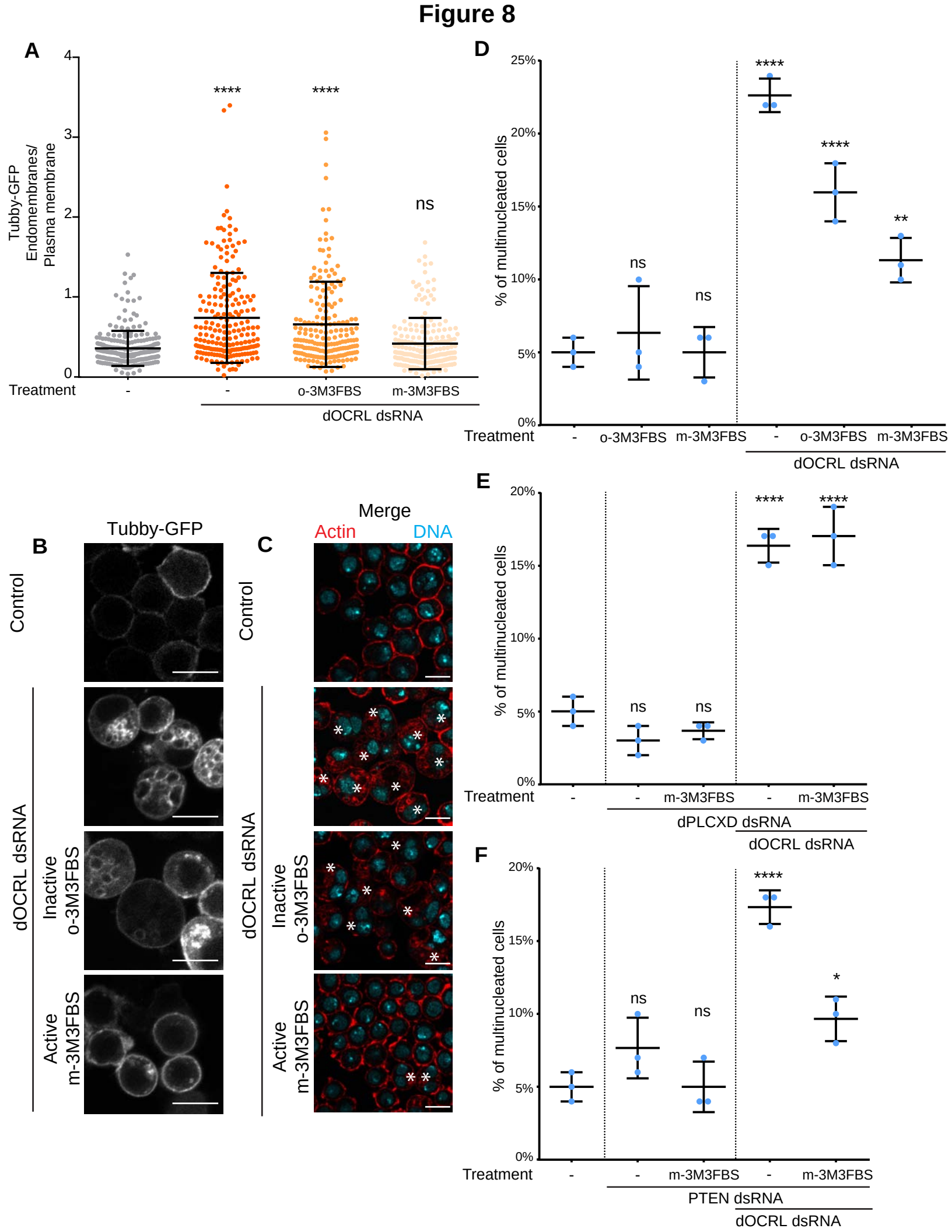
A
Tubby-GFP
Endomembranes/
Plasma membrane
0
1
2
3
4
****
****
ns
Treatment
-
-
o-3M3FBS
m-3M3FBS
dOCRL dsRNA
B
Tubby-GFP
C
Merge
Actin
DNA
Control
dOCRL dsRNA
Inactive
o-3M3FBS
Active
m-3M3FBS
D
% of multinucleated cells
0%
5%
10%
15%
20%
25%
ns
ns
****
****
**
Treatment
-
o-3M3FBS
m-3M3FBS
-
o-3M3FBS
m-3M3FBS
dOCRL dsRNA
E
% of multinucleated cells
0%
5%
10%
15%
20%
ns
ns
****
****
Treatment
-
-
m-3M3FBS
-
m-3M3FBS
dPLCXD dsRNA
dOCRL dsRNA
F
% of multinucleated cells
0%
5%
10%
15%
20%
ns
ns
****
*
Treatment
-
-
m-3M3FBS
-
m-3M3FBS
PTEN dsRNA
dOCRL dsRNA

Figure 9

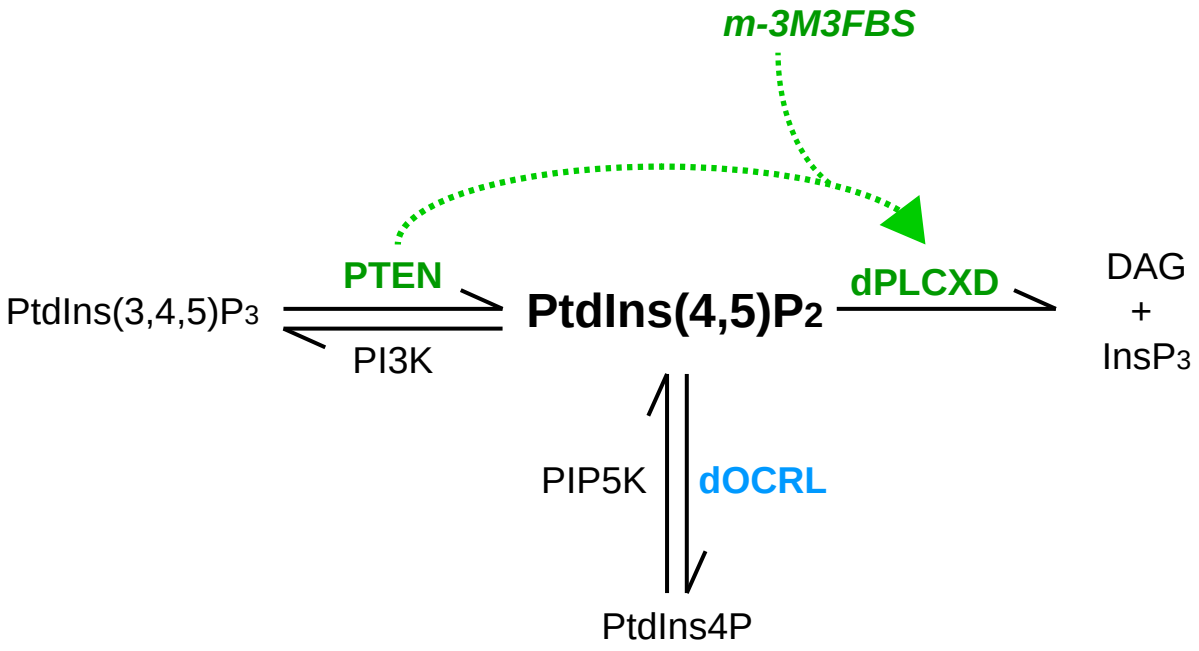
m-3M3FBS
PTEN
PtdIns(3,4,5)P3
PI3K
PtdIns(4,5)P2
dPLCXD
DAG
+
InsP3
PIP5K
dOCRL
PtdIns4P

Figure 10

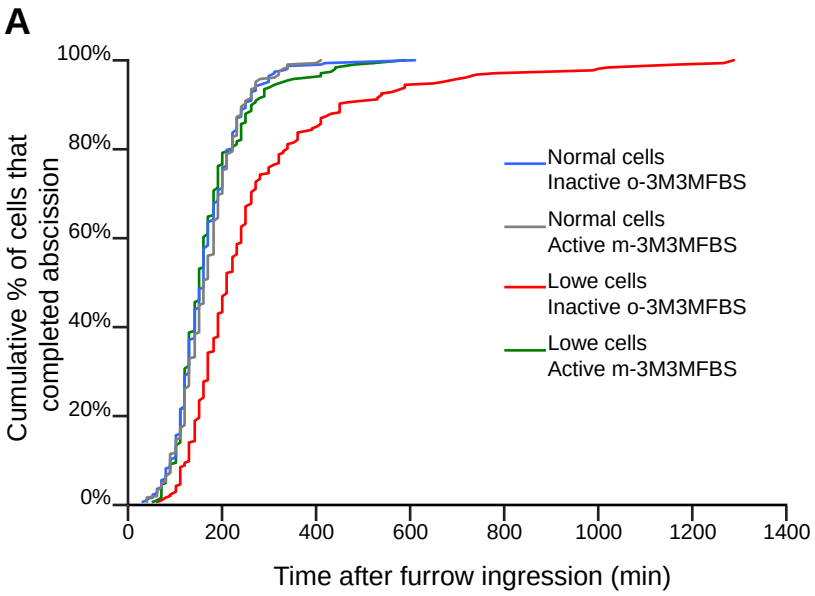
A
100%
80%
60%
40%
20%
0%
Cumulative % of cells that completed abscission
0
200
400
600
800
1000
1200
1400
Time after furrow ingression (min)
Normal cells
Inactive o-3M3MFBS
Normal cells
Active m-3M3MFBS
Lowe cells
Inactive o-3M3MFBS
Lowe cells
Active m-3M3MFBS

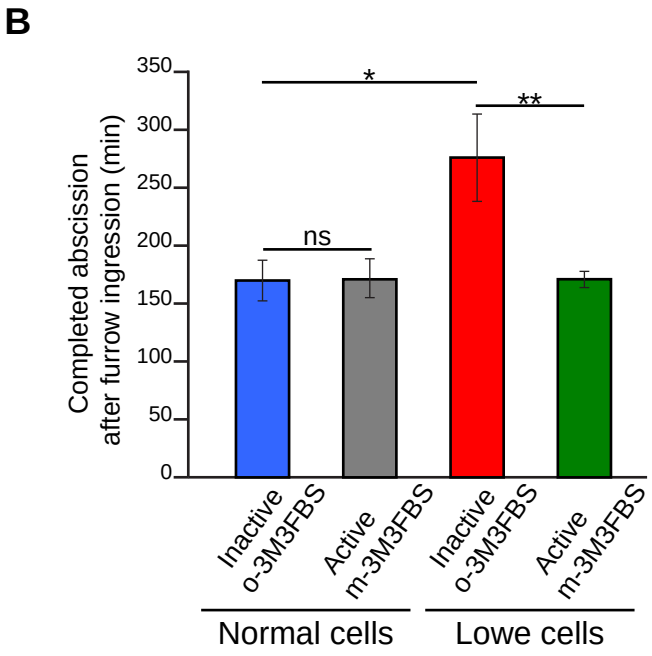
B
350
300
250
200
150
100
50
0
Completed abscission after furrow ingression (min)
*
**
ns
Inactive o-3M3FBS
Active m-3M3FBS
Inactive o-3M3FBS
Active m-3M3FBS
Normal cells
Lowe cells

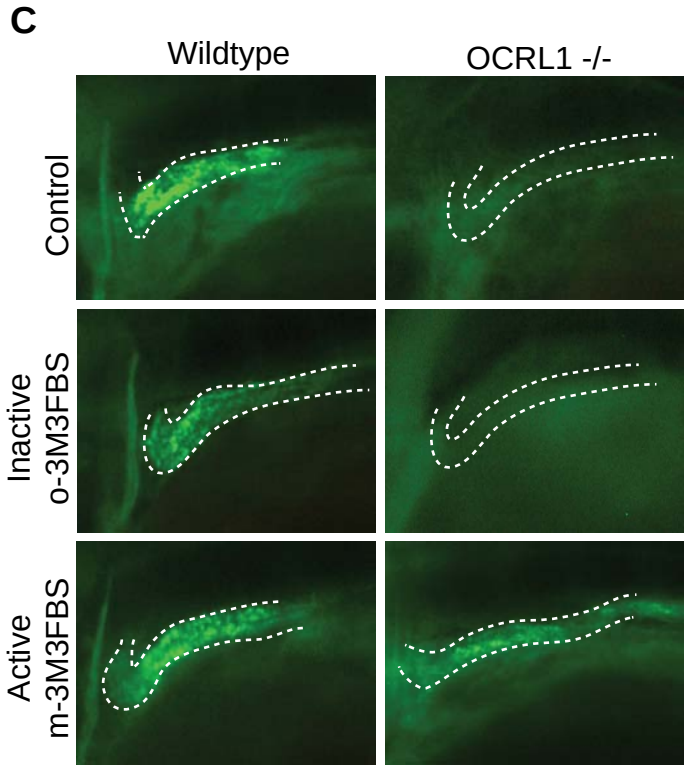
C
Wildtype
OCRL1 -/-
Control
Inactive o-3M3FBS
Active m-3M3FBS

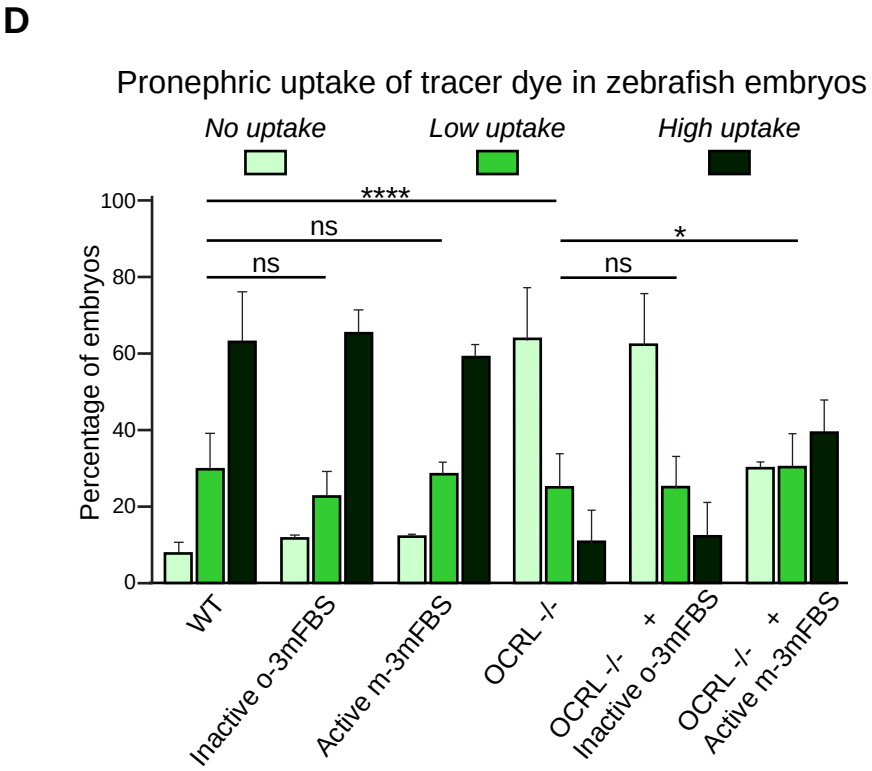
D
Pronephric uptake of tracer dye in zebrafish embryos
No uptake
Low uptake
High uptake
100
80
60
40
20
0
Percentage of embryos
****
ns
ns
ns
*
WT
Inactive o-3mFBS
Active m-3mFBS
OCRL -/-
OCRL -/- + Inactive o-3mFBS
OCRL -/- + Active m-3mFBS